Photophysical Studies of Zinc and Indium Tetraaminophthalocyanines in the Presence of CdTe Quantum Dots

A thesis submitted in fulfillment of the requirements

for the degree

of

MASTERS IN SCIENCE

of

RHODES UNIVERSITY

By

Jonathan Britton

January 2010

Abstract

CdTe QDs capped with mercaptopropionic acid (MPA) and thioglycolic acid (TGA) were covalently linked to zinc and indium tetraaminophthalocyanines (TAPcs) using N-ethyl-N(3-dimethylaminopropyl) carbodiimide (EDC) and N-hydroxy succinimide (NHS) as the coupling agents. The results presented give evidence in favour of formation of an amide bond between the MTAPc and CdTe QDs. Both the linked ZnTAPc–QD complexes and the mixture of QDs and ZnTAPc (without chemical linking) showed Förster resonance energy transfer (FRET), though the linked showed less FRET, whereas the QD interactions with InTAPc yielded no evidence of FRET. Both MTAPcs quenched the QDs emission, with quenching constants of the order of 10^{3}–$10^{4}M^{-1}$, binding constants of the order of 10^{8}-$10^{10}M^{-1}$ and the number of binding sites for the MTAPc upon the QD being 2. High energy transfer efficiencies were obtained (in some cases as high as 93%), due to the low donor to acceptor distances. Lastly, both MTAPc were shown to be poor optical limiters because their imaginary third-order susceptibility ($Im[\chi^{(3)}]$) was of the order of 10^{-17}-10^{-16} (optimal range is 10^{-9}-10^{-11}), the hyperpolarizability (γ) of the order of 10^{-37}-10^{-36} (optimal range is 10^{-29}-10^{-34}) and the k values were above one but below ten.

Table of Contents

List of Symbols

α - non-peripheral position

β - peripheral position

- nonlinear absorption term

ε - molar extinction coefficient

ε_S - singlet state molar extinction

ε_T - triplet state molar extinction

n - refractive index

Φ_{ISC} - inter system crossing quantum yield

Φ_F - fluorescence quantum yield

Φ_T - Triplet quantum yield

σ_{ex} - absorption cross section of the excited state

σ_g - absorption cross section of the ground state

Im[$\chi^{(3)}$] – imaginary component of the third order susceptibility

k - ratio of the absorption cross section of the singlet and triplet states

f - f is Lorentz local field factor

S_0 - ground singlet state

S_1 - excited singlet state

T_1 - first excited triplet state

T_n - nth excited triplet state

N_A - Avogadro's constant

ω* - frequency

F - Fluorescence intensity

F_0 - Fluorescence intensity in the absence of a quencher

J - Degree of spectral overlap of donor emission and acceptor absorption spectra

Eff - Efficiency of energy transfer

k^2 - Dipole orientation factor

$\mathbf{k_b}$ - Binding constant

r - Centre to centre separation distance between donor and acceptor

$\mathbf{R_0}$ – Förster distance

$\mathbf{^3O_2}$ – triplet state oxygen

$\mathbf{^1O_2}$ – singlet state oxygen

K – quenching constant

$\mathbf{I_{lim}}$ – limiting intensity

$\mathbf{Re[\chi^{(3)}]}$ – real component of the third order susceptibility

γ - hyperpolarizability

List of Abbreviations

Pc – Phthalocyanine

QD – Quantum Dot

DBU - 1,8-diazabicyclo[5.4.0] undec-7-ene

NHS - N-hydroxysuccinimide

EDC - N-(3-dimethylaminopropyl)-N'-ethylcarbodiimide hydrochloride

DMSO – dimethylsulfoxide

DMF - N,N'-dimethylformamide

NaOH - sodium hydroxide

1-CNP - 1-chloronaphthalene

TGA - thioglycolic acid

MPA - Mercaptoproprionic acid

ZnTAPc – Zinc tetraaminophthalocyanine

ClInTAPc – Indium (III) tetraaminophthalocyanine

CdTe – Cadmium Telleride

H_2Pc - metal-free phthalocyanine

^{1}H-NMR - proton nuclear magnetic resonance

HOMO - highest occupied molecular orbital

LUMO - lowest unoccupied molecular orbital

NLO - nonlinear optics

- nonlinear optical

MPc – metallophthalocyanine

IR – infrared

PDT - photodyanamic therapy

RSA - reverse saturable absorption

UV/Vis - ultraviolet/visible

FRET - Förster resonance energy transfer

IC - Internal conversion

MTAPc – Metallotetraaminophthalocyanine

XRD - X-ray powder diffraction

AFM - atomic force microscopy

TEM - transmission electron microscopy

BET - Brunauer Emmett Teller technique

STM - scanning tunnelling microscopy

SEM - scanning electron microscopy

Abs. – Absorption

A - Absorption

Fluor. – Fluorescence

ISC – Intersystem Crossing

Phosph. – Phosphorescence

Std. – Standard

Mix – Phthalocyanine and quantum dot mixed together

Link – phthalocyanine and quantum dot linked together

TS – tetrasulfonated

TC - tetracarboxy

OC - octacarboxy

Cys – cysteine

List of Figures

List of Tables

List of Schemes

Chapter 1

1. Introduction

1.1 Phthalocyanines

1.1.1 Introduction and General Applications

Phthalocyanines (Pcs) were discovered by chance in 1907 by Braun and Tcherniac. The brightly coloured compound, blueish in colour, was a by-product of synthesis of o-cyanobenzamide from phthalamide [1, 2]. Twenty years later, other phthalocyanine (Pc) derivatives were again obtained from the synthesis of phthalonitriles from o-dibromobenzene and cuprous cyanide by de Diesbach and von der Weid [3]. The structure of the metal free, unsusbstituted Pc was determined only about a quarter of a century later by the comprehensive research of Linstead and co-workers [4 - 7]. Linstead was the first to use the term phthalocyanine [4] which was derived from the Greek words *naphtha* (rock oil) and *cyanine* (blue), while the X-ray diffraction analysis of Pcs were carried out by Robertson and co-workers [8-10].

A Pc molecule is a planar macrocycle with an 18 π- electron system (see Fig. 1). The structure of Pcs grants them their renowned stability, both chemical and thermal. The pyrrole nitrogen atoms form a cavity into which metal ions can be incorporated [11]. More than seventy metals/metalloids can be (and have been) incorporated in the phthalocyanine core.

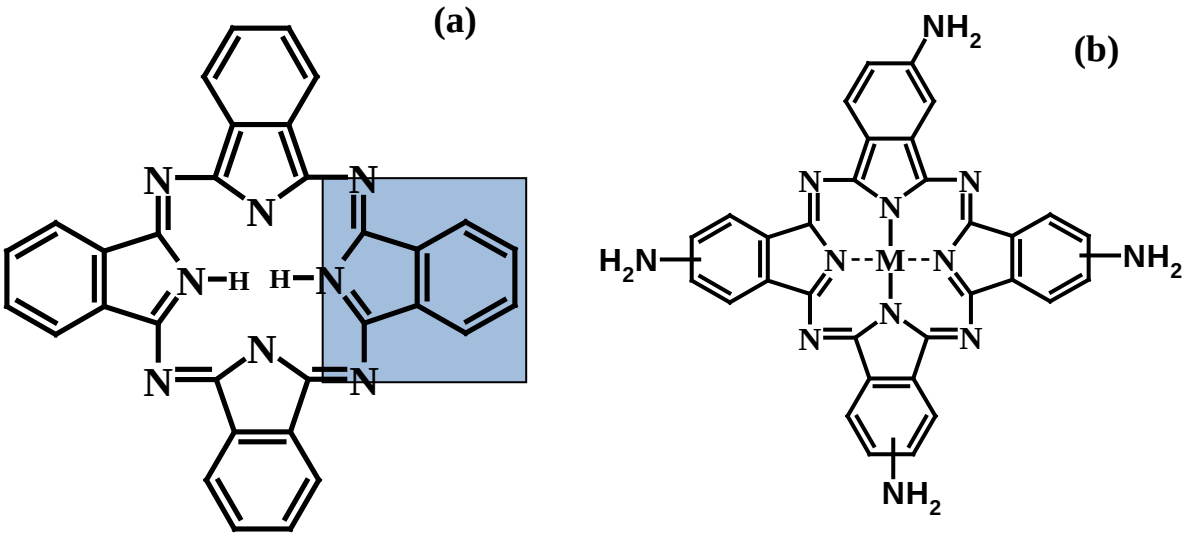

Fig. 1: (a) Indication of the four units which constitute a phthalocyanine's structure. (b) Structure of Metallotetraaminophthalocyanine.

Phthalocyanines have already been used for a diverse array of applications. Copper phthalocyanines are used as dyes in the textile and paper industry. Phthalocyanines are also used in high-speed CD-R media and often act as the donor molecule in organic solar cells. Probably the most significant application of phthalocyanines is in photodynamic therapy.

Photodynamic therapy (PDT) is a form of cancer treatment which involves a photosensitizer, a light source and oxygen present around the cancerous tissue. The photosensitizers most used are porphyrins and phthalocyanines, due to the fact that they are able to remain in cancerous tissue for a long time and that they can be engineered to posses the necessary energy requirements to produce singlet oxygen.

1.1.2 Tetraaminophthalocyanines

Metallotetraaminophthalocyanines (MTAPc), Fig. 1b, have in the past been predominantly used in creating modified electrodes for electrochemical analysis [12] of a variety of analyses, including pesticides, herbicides and insecticides. Aside from the fact that phthalocyanines have interesting and modifiable electrical properties, and are stable against light, heat and certain harsh environments, the amino groups seem to aide in the formation of TAPc polymers upon the chosen electrode surface. Along with this TAPcs are also able to form an amide bond with another compound which has a carboxylic acid group. Thus with the increased interest in nanoparticles, an opportunity to form phthalocyanine-nanoparticle conjugates using TAPcs presents itself, thereby linking the potentials of both molecules together and perhaps creating a more synergistic behaviour between the two. This is the aim of this work.

1.1.3 General Synthesis of Phthalocyanines

Phthalocyanines are synthesized through the cyclization of four benzene derivatives to form the planar macrocyle.

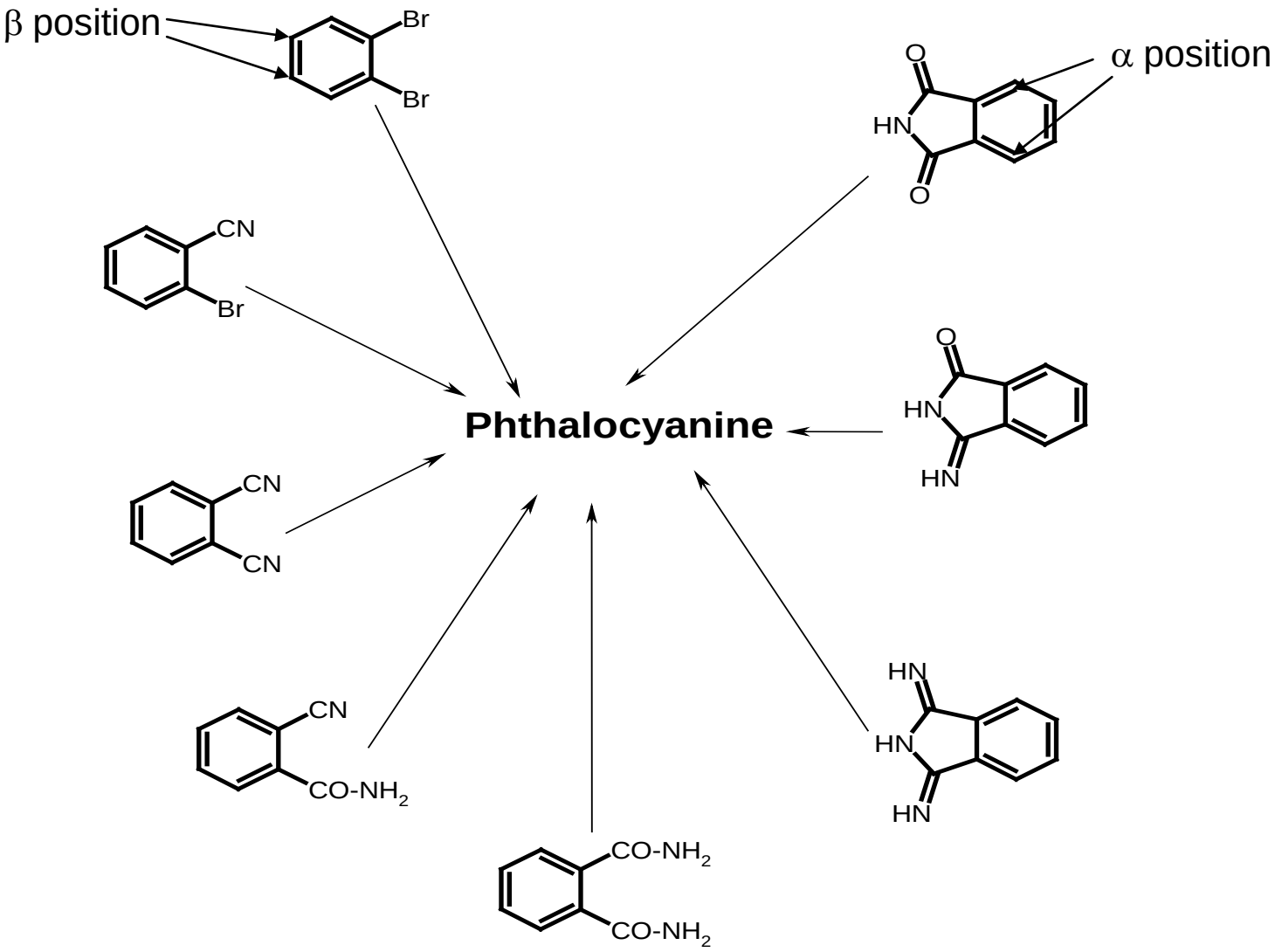

Scheme 1: Possible benzene derivatives used for Pc synthesis.

Benzene derivatives capable of forming Pcs, are shown in Scheme 1.

This is only a generalized synthetic route for phthalocyanines, and it is possible to modify the benzene derivative by binding a constituent onto either the α or β positions of the molecule (see Scheme 1). The binding of the constituent is actually accomplished through a nucleophilic substitution reaction, where generally either a halide or a nitro group is initially bound to the benzene derivative and then later substituted by the desired group. The halide or nitro group tends to draw electrons to itself, leaving the carbon vulnerable to attack from a nucleophile, which the

replacement group usually is. Thus MTAPcs are synthesized using the phthalonitrile route in Scheme 1.

1.1.4 Phthalocyanine Absorption Spectrum

A metal free phthalocyanine, H_2Pc, has a square planar, D_{2h} symmetry and C_2 axes in the x, y and z directions. When a metal is incorporated into the phthalocyanine cavity, the symmetry increases from D_{2h} to D_{4h}. This means that a metallated phthalocyanine has a D_{4h} symmetry. The increase in symmetry results in the reduction of allowed transitions.

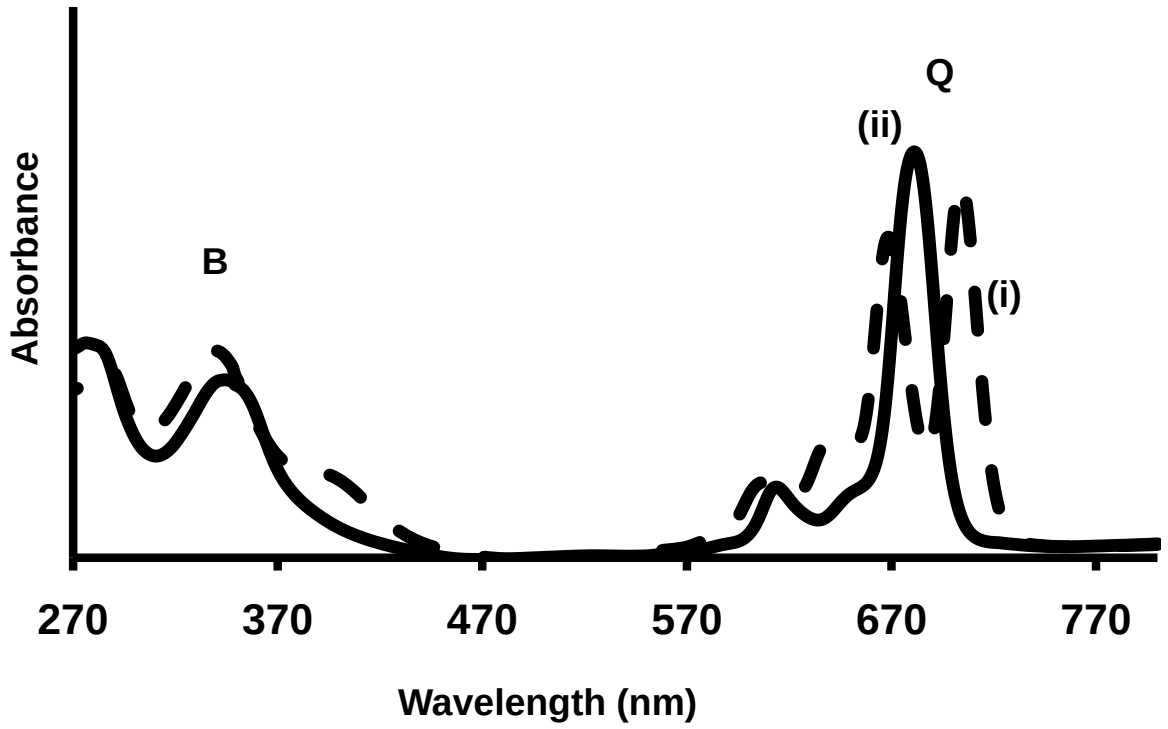

Fig. 2: Ground state electronic absorption of an unmetallated phthalocyanine (i) and metallated phthalocyanine (ii)

Metallophthalocyanines (MPcs) are known for their distinctive, strong absorption in the visible region of the spectrum (~ 670nm), called the Q band and weaker,

broader, absorptions at around 350nm called the B bands [13], Fig. 2, courtesy of B_1 and B_2. The assignment of the Q and B bands are based on the four-orbital model (Fig. 3), proposed by Gouterman's group [13-15]. The Q and B bands come from π - π * transitions and can be best explained in terms of a linear combination of transitions from a_{1u}, a_{2u} and b_{2u}, the highest occupied molecular orbitals (HOMO) of the MPc ring to the lowest unoccupied molecular orbitals (LUMO), e_g*. The low symmetry of an unmetallated Pc results in the splitting of the Q band (Fig. 2).

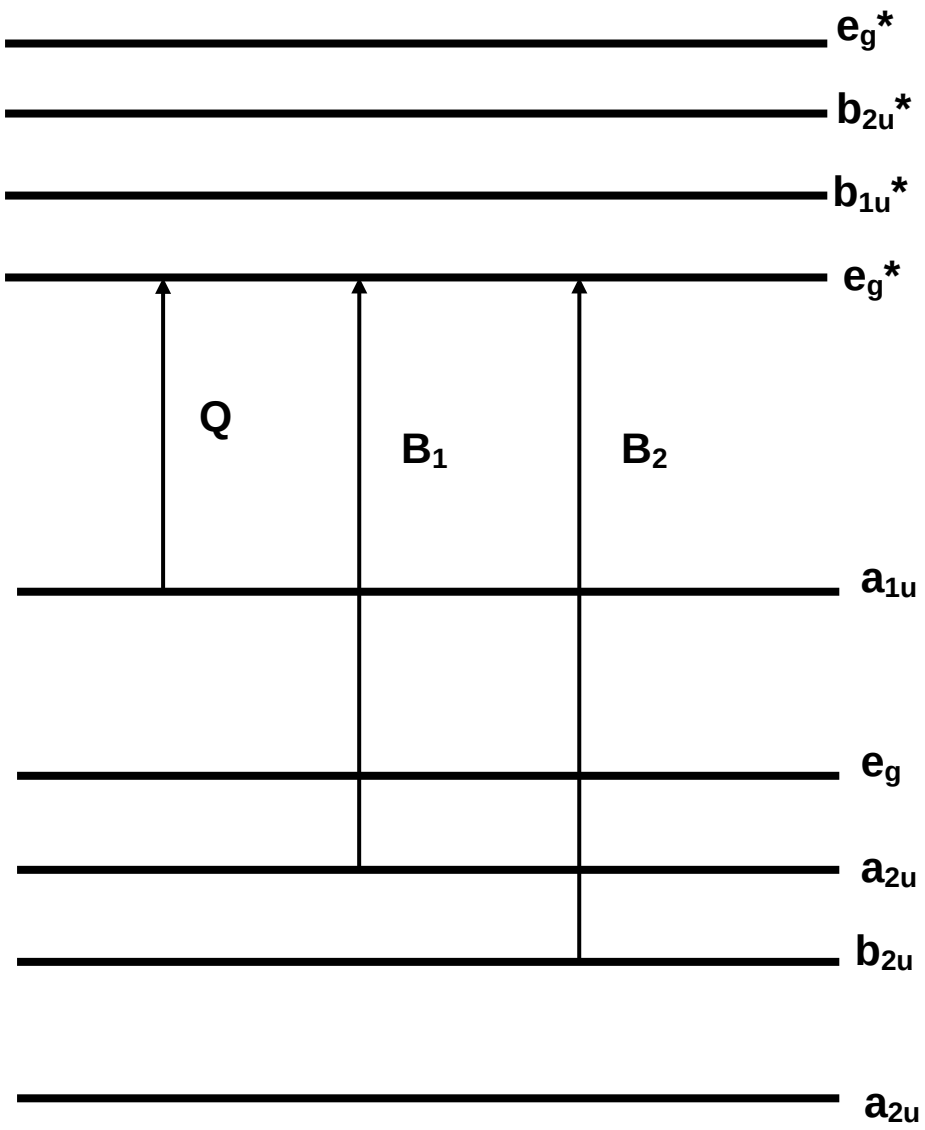

Fig. 3: Electronic transitions in phthalocyanines

There are other bands which are characteristic of MPcs, namely the N, L and C bands which will not be discussed in great detail here. These are found at higher energies (below 300 nm) in the ground state electronic absorption spectra and are primarily due to π - π* transitions [16].

1.2 Quantum Dots

1.2.1 Introduction

Quantum dots (QDs) are semiconductor nanocrystals that range in diameter size in the nanometer. Their size is smaller than the exciton Bohr radius of the bulk semiconductor material which the quantum dot is constructed, thus enabling confinement of an exciton in all three dimensions, and QDs are therefore considered dimensionless. The energy levels of the semiconductor nanocrystals now become discrete (Fig. 4), as compared to the valence and conductance bands which exist when the semiconductor is in its bulk form. What this ultimately means is that the quantum dots have numerous discrete energy levels that they can occupy when excited, usually by a photon of light, giving the quantum dot a rather broad absorption spectrum. However, the quantum dot can only emit energy as fluorescence from the lowest energy level in the conductance band to the highest energy level in the valence band. This means that the emission of a quantum dot is very specific and very narrow [17, 18] (Fig. 5).

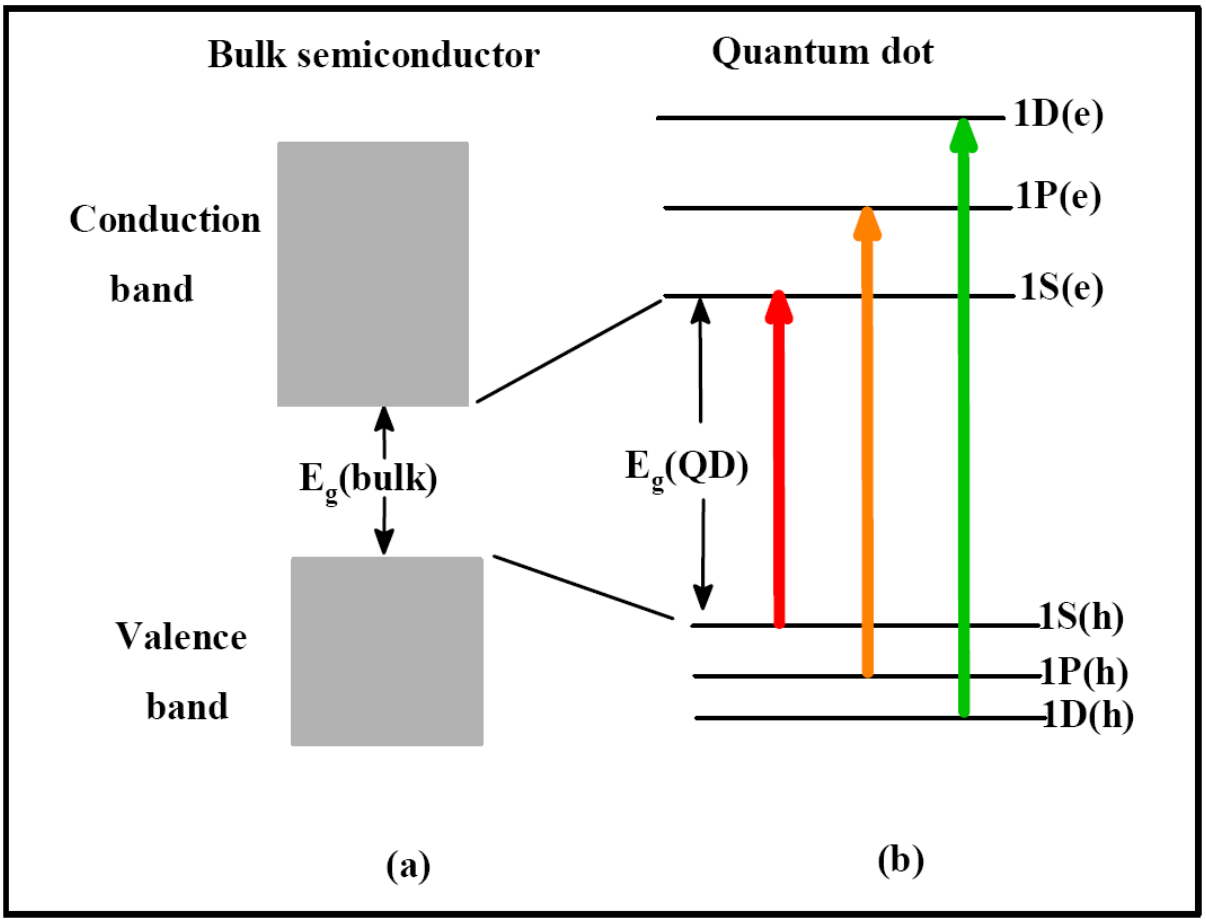

Fig. 4: Band gap in bulk crystals and QDs showing (a) continuous conduction and valence energy bands separated by a "fixed" energy gap, E_g(bulk) (b) QD characterized by discrete atomic-like states with energies that are determined by the QD radius [18].

Another effect of the exciton quantum confinement is that the energy gap between the conductance and valence bands initially increases for the smaller quantum dots, therefore blue-shifting the emission wavelength of the original bulk semiconductor. As the quantum dots grow in size and begin to assume a structure that more closely resembles the bulk's structure, the energy gap progressively decreases, thus red-shifting the emission. This is useful because it means that the quantum dots' emission region can be tuned to where it can be most useful [17-24].

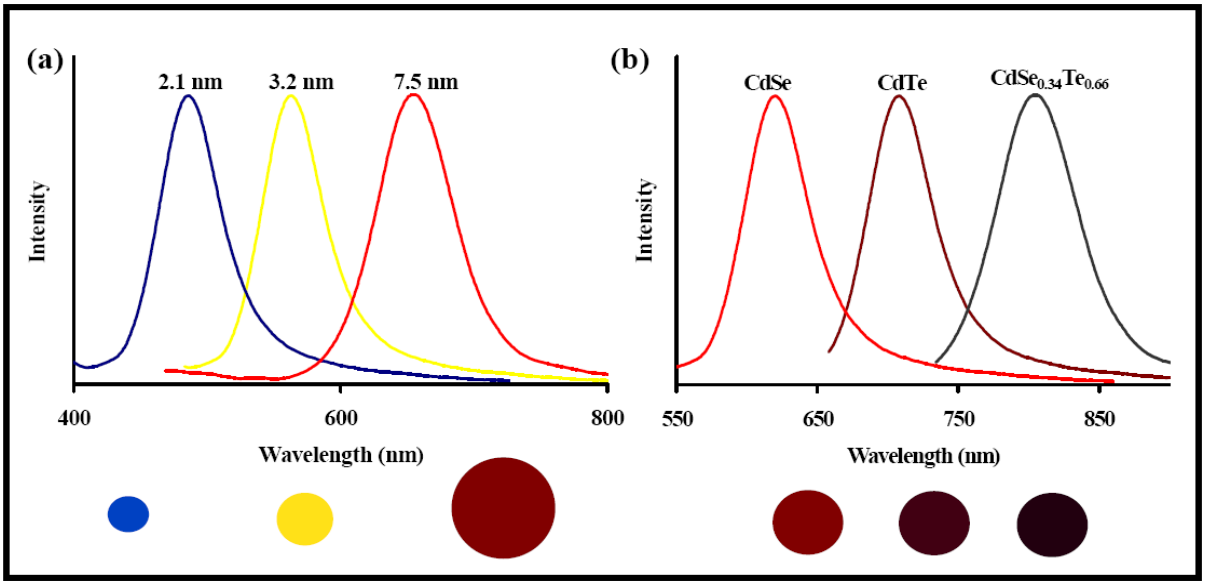

Fig. 5: QD emission wavelength tuned by changing the nanoparticle (a) size or (b) composition [18].

QDs have evolved a great deal since their initial creation in the early 1980s [25]. Where mainly CdTe and CdSe QDs were being made, QDs can be created with nearly every semiconductor in existence, as well as with many metals and insulators. Along with the expansion of the types of atoms which may be involved in the formation of the QDs, there are also many different techniques to creating QDs from one, two or three types of atoms in many differing ratios, as well as the possibility to create a “quantum dot shell” around an existing quantum dot [25].

While all these possibilities for QD formation do exist, there does appear to be a favouring of the combination of group III and group V elements and the group II and IV elements. In addition, since many QDs are formed from semiconductors, the possibility of doping the QD exists, which may add unique properties to the QD or merely enhance pre-existing ones [26].

QDs are capped during synthesis to stabilize them and helps regulate the growth. Capping can also help “trap” the QD’s atoms within its structure. To elaborate, the

capping agent is bound around the surface of a QD, effectively encapsulating it (bar a few defects which may arise). This makes it rather unlikely that an atom or ion from the QD lattice will escape into the surrounding environment it finds itself in. An added benefit of the capping agent is that depending on the structure of the capping agent used, different properties may be incorporated into the QD. These can range from water solubility to giving the QD terminal groups which may be used to create bonds with other molecules.

Quantum dots themselves have some ability to create singlet oxygen and radicals, meaning that they may be used for photodynamic therapy (PDT) to a certain degree as well, and, with their much broader absorption spectrum, excitation should be significantly easier and more flexible compared to the narrow absorption regions present in phthalocyanines for example [24, 27, 28]. However, unless the QD can be cleared quickly from the body, it is likely that the capping agent will end up degrading, leaving a “naked” QD within the body which may do more harm than good [24].

1.2.2 Water Soluble Quantum Dot Synthesis

There are generally two different pathways towards producing quantum dots referred to as the top-down and bottom-up approaches. Basically, one can either build up quantum dots from atoms or break down lattices to form them. Within the top-down pathway there exists two methods, both of which will be mentioned in a rather generalized sense. One method involves progressively confining the exciton of a lattice until it cannot move in any dimension (which is the definition of a QD). In this way quantum wells (which have the exciton confined in one dimension) and quantum wires (which confines the exciton in two dimensions) are also formed [25].

A second method involves a “self-assembled” approach. This works by utilizing a difference in the lattice constants of two semiconductors, where the lattice constant represents the distance between atoms in ordered crystalline structures. This results in a process termed strained epitaxial growth, and this method has been used to create GeSi QDs as well as to form InAs around GaAs QDs [25].

The bottom-up method is the most well established of the methods, having originated in the 1980s [25], and this is the method used to synthesize the QDs used in this thesis. The process involves the initial combination of the cadmium, tellurium and capping agent, called nucleation, followed by the heating of the solution to grow the QDs to the desired size, a process called Ostwald ripening. The tellurium is usually introduced as a hydrogen telluride gas, but an alternate approach is the use of a sodium hydrogen telluride solution, which is produced by the stirring of tellurium powder and sodium borohydride in a small amount of deionised water.

The water soluble nature of a quantum dot is determined by the type of capping agent used. In this work, for example, mercaptoproprionic acid (MPA) and thyoglycolic acid (TGA) were used because the end in a carboxyl group, thus meaning that the resultant QDs would be water soluble. Amino groups also work, though the pH used for this synthesis would be lower than the pH 11 used for MPA and TGA.

1.2.3 Quantum Dot Size Characterization

QDs may be characterized using UV-Vis spectroscopy, X-ray powder diffraction (XRD), atomic force microscopy (AFM), transmission electron microscopy (TEM) and the Brunauer Emmett Teller (BET) technique, to name a few. With UV-Vis

spectroscopy, only the size of CdTe quantum dots can be estimated using the polynomial fitting function derived in the literature [29], equation 1:

$$D = (9.8127 \times 10^{-7})\lambda^3 - (1.7147 \times 10^{-3})\lambda^2 + (1.0064)\lambda - (194.84) \quad (1)$$

where λ is the absorption maxima of the QDs. When using XRD, size may be confirmed using the Scherrer equation 2:

$$d(\text{Å}) = \frac{k\lambda}{\beta Cos\theta} \quad (2)$$

where k is an empirical constant equal to 0.9, λ is the wavelength of the X-ray source, (1.5405 Å for Cu), β is the full width at half maximum of the diffraction peak, and θ is the angular position of the peak.

Some other available methods include AFM, scanning tunnelling microscopy (STM), TEM and scanning electron microscopy (SEM). Whilst all of these techniques operate on different principles, the method each use for size determination is the same and that is the comparison of the diameter of an image of a quantum dot to a determined scale for the image. The only real difference between them is resolution and operation speed. For example, SEM is faster than TEM, but also has about 40 times lower resolution than TEM, and cannot be used with samples smaller than 30Å. Another issue which can arise, especially in AFM, is the aggregation of the quantum dots together, thus making them appear larger than they actually are. Lastly, all of these techniques generally only look at a small region of the total sample and the quantum dot sizes present there, whereas XRD which will give an average size for the entire sample [30].

BET is also useful for QD size determination. The amount of gas adsorbed onto the QD to form a monolayer is determined. Used with the cross-sectional area that the gas particles occupy, the QD diameter can be calculated as an average, though it

tends to give larger values than other techniques and the result can also be disrupted due to aggregation of the QDs [31-33].

Photoluminescence and photoluminescence excitation are also possible size determination techniques, though it is unclear exactly how this technique operates. There seems to be some involvement of the luminescence intensity as an indicator of particle size, with the argument being that nanoparticles contain fewer defects to quench their luminescence than the bulk material does. Also, the luminescence would give an indication of the energy band gap of the particle, so perhaps these factors are used together to determine size [30].

Lastly, two techniques that could be used appear to operate in the same manner as XRD, in that scattering patterns obtained are used to determine the particle's size. These two techniques are Raman scattering spectroscopy and dynamic light scattering [30]. In this work XRD and the polynomial equation are employed to determine the size of the QDs synthesized.

1.2.4 Linking of QD to MPc

Though QDs have been around for about 30 years, very little work has been done on them until recently, where, due to their strong fluorescence, they have found application in biomedical imaging in the body. They are especially effective when they are linked to a compound which is naturally drawn to a cell of interest, such as certain antibodies.

In terms of this work, amino groups offer a point of attachment for the mercaptoproprionic acid and thioglycolic acid capping agents used to form water soluble QDs, both of which end in a carboxylic acid group. The idea is to use the linking agents N-ethyl-N(3-dimethylaminopropyl) carbodiimide (EDC) and N-hydroxy

succinimide (NHS) to form an amide bond between the phthalocyanine and the QD (see Scheme 2), with the end result being that the QD is attached to the phthalocyanine (Pc) molecule.

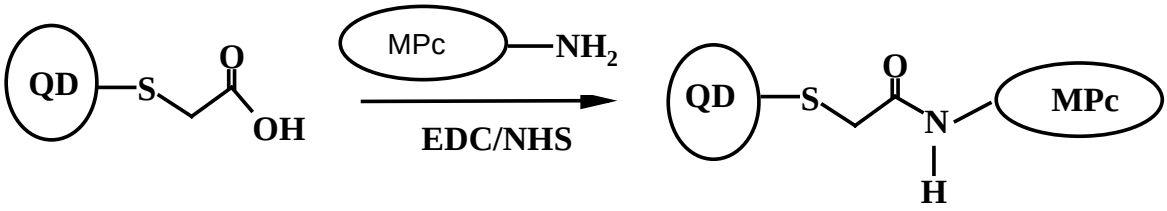

Scheme 2: Linking of QD to MPc with an amino group using EDC/NHS as coupling agents.

The issue with mixing the two is the fact that one cannot guarantee that both QD and Pc will end up in the cancer cells at the same time. It is therefore useful to attempt to link the two compounds so that they may travel together to the target. However, surprisingly little has been done in linking Pcs to QDs to date. This is probably due to initial focus being on the linkage of QDs to various antibodies and hormones, so as to enable the QDs to travel selectively to a particular type of cell for bio-imaging purposes [34]. This does not mean that no studies have been done on the linkage of Pcs to nanoparticles. One study deals with the linkage of a hydrophobic photosensitizer to a gold nanoparticle, and incubated with HeLa cells (a cervical cancer cell line), in order to make the photosensitizer more water-soluble [27]. Another paper examined four silicon phthalocyanines that were linked to CdSe through axial ligation, and the energy transfer was examined between the Pc and QD using a femtosecond laser [26] (Fig. 6).

Since most papers have dealt with axial linkages, linkage via the peripheral position is worth examination and is a first in this thesis.

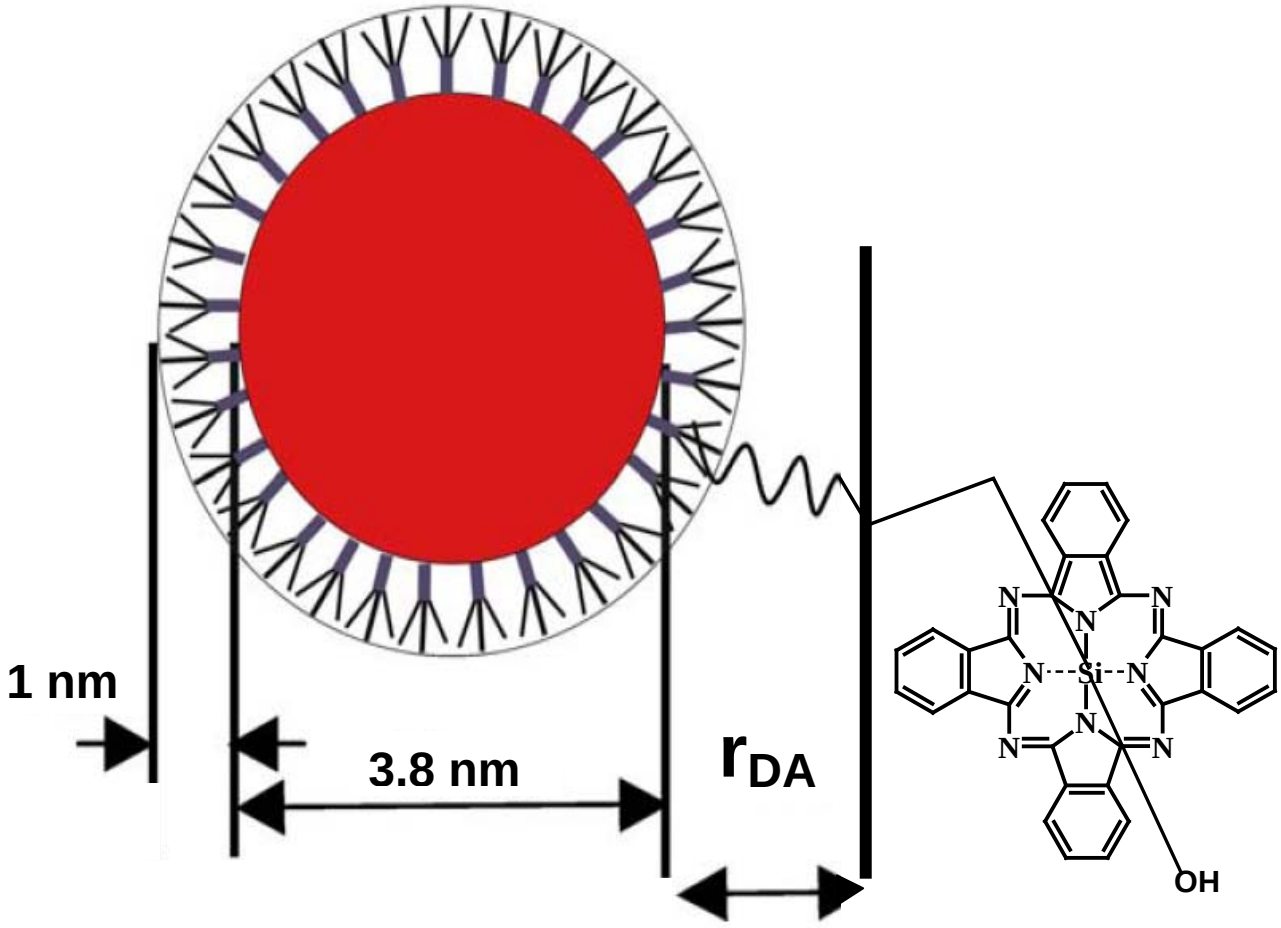

Fig. 6: CdSe-Pc conjugates [26].

1.3 Photophysics

A Jablonski diagram is a representative diagram of the energy transitions and spin alterations that electrons of a molecule can undergo. The triplet-triplet absorption is indicated by the T_1 to T_n transition, while the S_0 is the ground state (Fig. 7) of the molecule. S_0 to S_1 indicates absorption (abs.), whilst S_1 to S_0 is fluorescence (fluor.). The S_1 to T_1 transition represents intersystem crossing (ISC). Transition between the S and T levels involves an alteration in electron spin, which is ordinarily forbidden to happen but due to the closeness of the S_1 and T_1 energy levels and spin orbit coupling it becomes allowed.

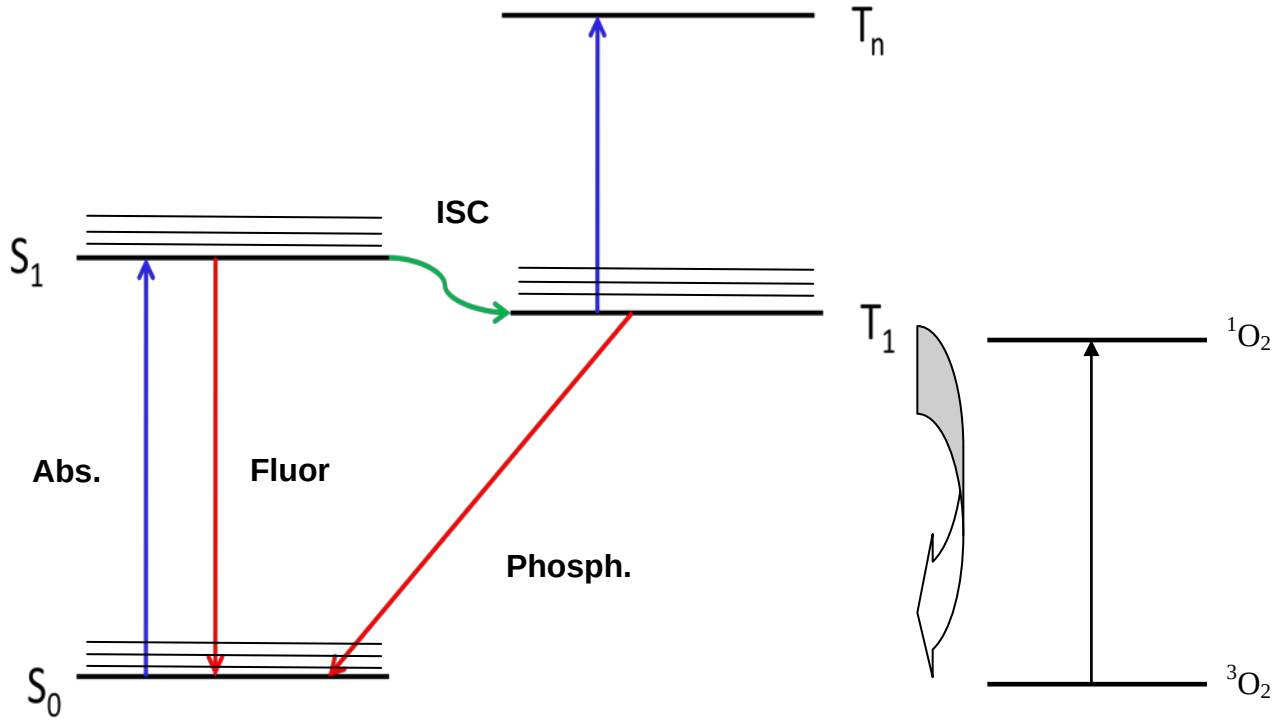

Fig. 7: Basic Jablonski diagram.

Phthalocyanines cause cancer cell death due to their ability to produce singlet oxygen, which can kill cells through apoptosis or necrosis. The singlet oxygen is

produced when energy from phthalocyanines in the triplet state is transferred to triplet oxygen (Fig. 7), forming singlet oxygen, whilst the phthalocyanines return to their singlet ground state. Due to the fact that phthalocyanines locate mainly around cancerous tissue, the damage the singlet oxygen does is only localized there.

1.3.1 Fluorescence Quantum Yields

The fluorescence quantum yield of a molecule gives an indication of the efficiency of the fluorescence process (or how many of the photons absorbed by the molecule are lost through emission), as well as an indication of the purity of the molecule, because impurities will tend to quench the target molecule's fluorescence. Fluorescence calculations are mostly done via a method of comparison of the sample's fluorescence to that of a standard using the following equation [35, 36]:

$$\Phi_F = \Phi_{F\,(Std)} \frac{F \,.\, A_{Std} \,.\, n^2}{F_{Std} \,.\, A \,.\, n^2_{Std}} \qquad (3)$$

where F is the fluorescence peak area of the sample and standard, A is the absorption of the sample and standard at a particular wavelength and Φ_F is the fluorescence quantum yield of the sample and standard. Std = Standard; n = refractive index.

The standard most often employed for phthalocyanine fluorescence quantum yield calculations is zinc phthalocyanine in a particular solvent (because, as the equation indicates, the refractive indices of the solvents that the sample and standard are in, do play a role in determining the ultimate fluorescence quantum yield value for the sample). In addition zinc phthalocyanine also has good absorption spectrum overlap with other phthalocyanines, but it is possible to use other standards if they possess a

superior overlap to zinc phthalocyanine. The absorbance values of the sample and standard are also set to the same intensity at the wavelength the fluorescence measurement is to be carried out at, so as to have the sample and standard at a similar concentration.

When calculating the fluorescence quantum yields for QDs alone, Rhodamine 6G in ethanol is used as the standard instead of the zinc phthalocyanine. The fluorescence quantum yield of the quantum dot alone is needed in order to calculate the fluorescence quantum yields of the QD mixed or linked to a phthalocyanine, using the following equations [19, 37]:

$$\Phi_{F(QD)}^{Mix} = \Phi_{F(QD)} \frac{F_{QD}^{Mix}}{F_{QD}} \quad (4a)$$

$$\Phi_{F(QD)}^{Link} = \Phi_{F\,(QD)} \frac{F_{QD}^{Link}}{F_{QD}} \quad (4b)$$

where Φ_F is the fluorescence quantum yield of the QD alone and of it mixed or linked with the Pc, and F is the fluorescence intensity of the mixture, linked and QD alone. Mix = mixed; link = linked.

This is also a comparative method. It is more accurate to use QDs as a standard than Rhodamine in equations 4, since the QD structure can vary in terms of surface imperfections.

1.3.2 Triplet Quantum Yields and Lifetimes

The triplet quantum yield is an indication of how many molecules have entered the triplet state per photon of light absorbed. The triplet lifetime is obtained through laser

flash photolysis and OriginPro 7.5 software, and the triplet quantum yield is obtained using equation 5 [38]:

$$\Phi_T = \Phi_T^{Std} \frac{\Delta A_T \varepsilon_T^{Std}}{\Delta A_T^{Std} \varepsilon_T} \quad (5)$$

where ΔA_T and ΔA_T^{Std} are the changes in the triplet state absorbances of the MPc derivatives and the standard, respectively. ε_T and ε_T^{Std} are the triplet state molar extinction coefficients for the MPc derivatives and the standard, respectively. Φ_T^{Std} is the triplet quantum yield for the standard, e.g. ZnPc.

1.3.3 Förster Resonance Energy Transfer (FRET)

One of the areas in which a quantum dot could be effective is Förster Resonance Energy Transfer (FRET), where the quantum dot's energy is transferred to an acceptor molecule.

Molecules which have been used as receptors of this energy transfer are Pcs, with some studies focussing on the FRET which occurs between water-soluble CdTe QDs and either positively or negatively charged Pcs [21- 23]. This is an interesting study due to the fact that most capping agents which can make a QD water-soluble tend to make the QD negatively charged as well, along with the fact that Pcs are also photosensitizers used for cancer treatment. This means that the transferred energy can be used to produce singlet oxygen to destroy cancer cells, assuming that the two compounds are localized around the cancer cells, and that the wavelength of light used is suitable for PDT [24].

One of the problems with quantum dots (QDs) is the toxicity of the starting materials used in their syntheses. In particular, are the cadmium telluride and cadmium selenide QDs, which consist of cadmium and either tellurium or selenium, all of which are highly toxic, but these QDs emit in a region which makes them excellent FRET candidates with phthalocyanines.

Table 1: FRET Parameters of Referenced Compounds.

Compound	**J (x 10^{-13} cm^6)**	**R_0 (Å)**	**r (Å)**	**Eff (%)**	**[Ref]**
(1)-CdSe		17.4	18.1	44	[25]
(2)-CdSe		17.7	16.5	60	[25]
(3)-CdSe		17.6	15.3	70	[25]
(4)-CdSe		17.5	22.3	19	[25]
ZnTSPc+CdTe-TGA	18	57	67	30	[22]
ZnTCPc+CdTe-TGA	7.2	49	63	20	[22]
ZnOCPc+CdTe-TGA	7,9	50	60	20	[22]
(5)+CdTe-MPA	1.36	39.95	38.4	21	[21]
(5)+CdTe-TGA	1.17	35.47	44.20	21	[21]
AlTSPc+2.3nm CdTe-MPA	1.08	39.39	52.06	16	[39]
AlTSPc+3.7nm CdTe-MPA	8.20	72.81	68.99	58	[39]

AlTSPc+2.7nm CdTe-TGA	1.73	46.09	62.38	14	[39]
AlTSPc+3.6nm CdTe-TGA	9.75	69.21	76.73	35	[39]
AlTSPc+3nm CdTe-Cys	1.37	46.57	57.52	22	[39]
AlTSPc+3.5nm CdTe-Cys	13.9	44.69	25.04	97	[39]

TS = tetrasulfonated; MPA = mercaptoproprionic acid; TGA = thyoglycolic acid; TC = tetracarboxy; OC = octacarboxy; Cys = cysteine.

J = Spectral Overlap; r = centre-to-centre distance between donor and acceptor molecules; R_0 = Förster distance; Eff = FRET efficiency.

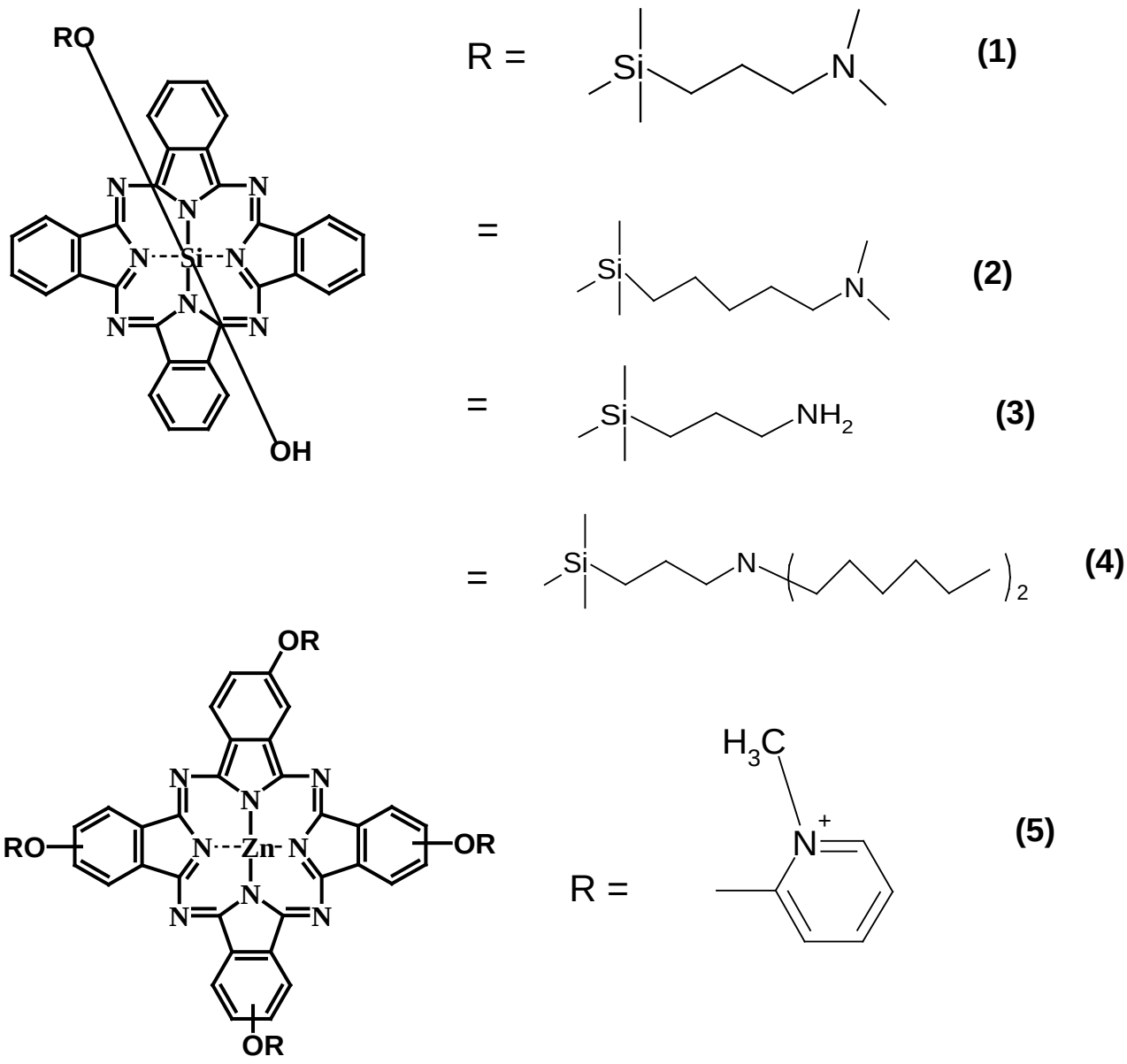

Fig. 8: Structure of Phthalocyanines (1)-(5).

Fig. 8 shows the structures of phthalocyanines **(1)**-**(5)** in Table 1. As can be determined from Table 1, only Pcs mixed with QDs or QDs linked axially to Pcs have been examined for FRET [21, 22, 25, 39], whereas this study will examine Pcs and QDs linked peripherally for FRET.

FRET has three factors which determine whether energy transfer would occur and how efficient the process is. The first is the spectral overlap, which allows one to

determine how close the energy of fluorescence of the donor is to the absorption of the acceptor. A smaller energy difference helps to bring about a more efficient FRET, and the amount of spectral overlap can be indicated with J [19, 28] (equation 6):

$$J = \int f_{QD}(\lambda)\, \varepsilon_{MPc}(\lambda)\, \lambda^4\, \partial\lambda \qquad (6)$$

where f_{QD} is the normalized QD emission spectrum; and ε_{MPc}, the molar extinction coefficient of MPc complexes. λ is the wavelength of the acceptor at the Q band.

The distance between two substances is also important, since better energy transfer is likely between substances that are close together than those that are further apart. The actual distance is calculated using equation 7 [19, 28]:

$$Eff = \frac{R_0^{\,6}}{R_0^{\,6} + r^6} \qquad (7)$$

where the r value is the centre to centre distance and the R_0 is the Förster distance and Eff is FRET efficiency.

The value of efficiency used in equation 7 is determined from equation 8, and it links the fluorescence quantum yields to the FRET parameters [19, 21, 28]:

$$Eff = 1 - \frac{\Phi_{F(QD)}^{Mix}}{\Phi_{F(QD)}} \qquad (8)$$

The Förster distance (R_0) is the distance at which 50% FRET efficiency occurs and is determined from the following equation 9 [19, 28]:

$$R_0^{\,6} = 8.8 \times 10^{23}\, \kappa^2\, n^{-4}\, \Phi_{F(QD)}\, J \qquad (9)$$

where κ^2 is the dipole orientation factor; n, the refractive index of the medium; $\Phi_{F(QD)}$, the fluorescence quantum yield of the donor in the absence of the acceptor; and J is the Förster overlap integral, defined by equation 6. k is usually difficult to determine accurately, due to the small nature of the substances involved, but in this case it is

assumed that κ^2 is 2/3; such assumption is often made for donor-acceptor pairs in a liquid medium, since their dipole moments are considered to be isotropically oriented during the excited state lifetimes.

Spectral overlap and Förster distance may be determined using a computer program called PhotoChemCAD [40].

Table 1 lists FRET parameters of MPcs in the presence of QDs, and shows J values to be of the order 10^{-13} cm^6. R_0 must be greater than r for efficient FRET (Eff. > 50%) and this is the case for only a few complexes in Table 1 (**(2)**-CdSe, **(3)**-CdSe and AlTSPc + 3.7nm CdTe-MPA QDs). Thus there are only a few MPc-QD mixtures which show high FRET efficiency. This work aims at improving FRET efficiency by linking QDs to MPCs using peripheral substituents.

1.3.4 Fluorescence Quenching Parameters

Much information about the interaction of two substances in a system can be obtained by observing how one system affects the other. This is also true for a QD-Pc system, where the QD emission is quenched due to an energy transfer to the Pc through FRET.

Thus the quenching constant (K) may be obtained using the following Stern-Volmer equation [41]:

$$\frac{F_0}{F} = 1 + K[MPc] \qquad (10)$$

where F_0 is the fluorescence of the QD in the absence of Pc and F is the fluorescence obtained through the various additions of Pc to the QD solution.

In terms of FRET analysis, knowledge about the rate of quenching gives an indication of which phthalocyanine is receiving the QD's energy more readily,

because the quenching experienced is a mixture of that energy transfer and any energy lost through internal conversion and heat given off through collisions between the particles.

Secondly, binding constants (k_b) and number of binding sites (n) on the QD may be determined by using a modified Stern-Volmer plot (equation 11):

$$\log\left[\frac{(F_0-F)}{(F-F_\infty)}\right] = \log k_b + n\log[MPc] \quad (11)$$

where F_0 is the fluorescence of the QD without Pc, F is the fluorescence of the QD with Pc and F_∞ is the fluorescence of the QD when saturated with Pc.

The binding constant gives an indication of the ease with which two substances form a linkage or perhaps how strong an affinity they have for one another. A value below one indicates a low affinity, while a value above one indicates various degrees of affinity for one another and a readiness to form a linkage. The number of binding sites gives an indication of how many molecules are bound to another [41].

1.4 Nonlinear Optics (NLO)

All matter possesses an electromagnetic field of varying intensities, and it is because of this field that matter and light are able to interact. Nonlinear optics is a branch of study of this interaction, more specifically how matter interacts with intense laser light. Higher intensity light can result in differing behaviour which does not occur when the light of a lower intensity is used with certain materials. As such, triplet quantum yield analysis can give information in this area.

Optical limiting is a specific branch of nonlinear optics, and it deals with how certain materials are able to regulate light intensity. This means that certain materials do not transmit light linearly at high intensities, but, instead, have a fixed intensity transmission, (Fig. 9). Fig. 9 merely represents the idea that the light transmitted by material A is the same intensity when both low and high intensity light is applied to it, indicating that the optical limiting response is arising from the triplet-triplet absorption (see Fig. 7) of A.

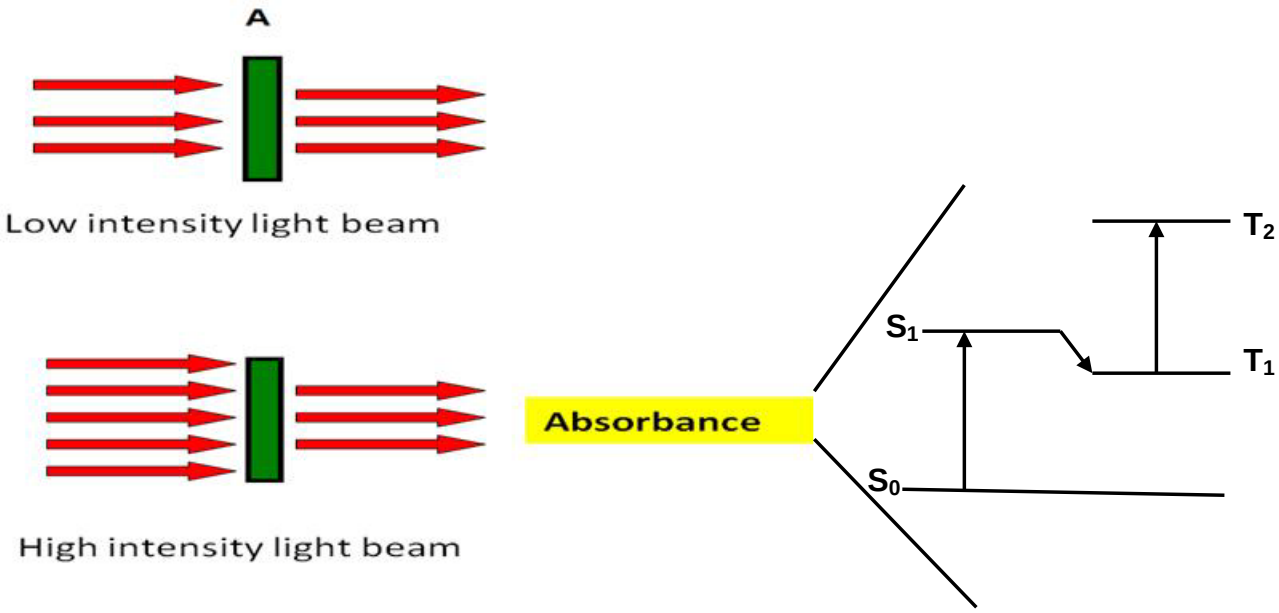

Fig. 9: Schematic representation of the ideal functioning of a phthalocyanine optical limiter under low and high intensity light.

This optical limiting phenomenon has been observed in both phthalocyanines and QDs, and in the case of phthalocyanines it is the triplet-triplet absorption (Fig. 7) which is responsible for the response.

1.4.1 Optical Limiting of Phthalocyanines

Both phthalocyanines and QDs are good candidates as optical limiters due to their tuneable nature and, in the case of phthalocyanines, their triplet-triplet absorption. The mechanism responsible for the optical limiting effect in QDs is not perfectly understood. Hence in this work only the MTAPcs will be studied for nonlinear optical limiting.

The phthalocyanines most used as optical limiters are those with heavy metals like indium, gallium, lead and antimony as the central metal, as well as those with peripheral groups that help with the solubility and disaggregation of the phthalocyanine. It is possible also to utilize the peripheral groups to minimize the singlet-singlet absorption around the area where the maximum triplet-triplet absorption occurs [42- 45].

Phthalocyanines have been used extensively as optical limiters due to the ease with which a Pc enters a triplet state, where the optical limiting behaviour originates from. Aside from the enhanced intersystem crossing, heavy metals tend to disrupt the Pcs original symmetry. This is because the heavy metals rarely fit into the Pc cavity and, instead, are held slightly above the ring, and this altered symmetry also appears to be beneficial to good optical limiting ability.

1.4.2 Nonlinear Optical Parameters

One of the more common methods for determining optical limiting parameters is the use of a z-scan, which essentially provides the nonlinear refraction and absorption directly from the device's measurements. These are the two major factors which help explain the processes involved in optical limiting.

This is not the only method which can be used though. Another involves the use of triplet quantum yield and triplet lifetime measurements in the calculation of these parameters. The first parameter is the limiting intensity (I_{lim}), which essentially indicates the intensity at which the optical limiting response will begin to occur, and it is done using equation 12 [46, 47]:

$$I_{\lim} = \frac{h\omega^*}{2\pi\sigma_{13}\tau_{21}} \qquad (12)$$

where ω^*, σ_{13} and τ_{21} are the frequency at which the system absorbs, singlet state absorption cross section and triplet lifetimes, respectively, and 1 = S_0, 2 = T_1 and 3 = S_1. There is no specified optimal range for I_{lim} values, however the lower they can be the better the optical limiter because the optical limiting behaviour will occur sooner.

The imaginary component of the third order susceptibility is also representative of the nonlinear absorption, with the real component being representative of the nonlinear refraction of the compound, equation 13:

$$\mathrm{Im}\left[\chi^{(3)}\right] = \frac{2c^2{\eta_0}^2\beta}{\pi\omega^*} x10^{-22} \qquad (13)$$

where η and c are, respectively, the linear refractive index, and the speed of light and ω^* is the frequency at which the system absorbs.

$$\beta = 5.3\varepsilon_S\varepsilon_T[C]\Phi_{\mathrm{ISC}} \qquad (14)$$

where ε_S and ε_T are extinction coefficients for the ground and triplet state, respectively, [*C*] is the concentration of active species in the triplet state and Φ_{ISC} is the intersystem crossing quantum yield [46,48], equation 14. The optimal range for $\mathrm{Im}[\chi^{(3)}]$ is 10^{-9}-10^{-11} [49].

It is not possible to calculate the real component of the third-order susceptibility directly, due to the fact that the equation does not contain easily measured elements. This is better illustrated by viewing equation 15 [46]:

$$\mathrm{Re}\left[\chi^{(3)}\right] = \frac{c{\eta_0}^2\eta_2'}{120\pi} x10^{-20} \qquad (15)$$

As can be seen in equation 15, the η_2 element is a nonlinear refraction term which is difficult to measure on its own. The real component is usually measured directly with the z-scan, but it is not essential, because the imaginary component usually yields more meaningful data on how effective an optical limiter the compound is [46].

Another term to consider is one called hyperpolarizability. Whilst the imaginary component of the third-order susceptibility of the compound gives the nonlinear absorption, it is for the whole solution. Hyperpolarizability gives the nonlinear

absorption per mole of compound, which is useful when it comes to comparison of the effectiveness of multiple compounds. Hyperpolarizability is calculated using equation 16 [46, 50]:

$$\gamma = \frac{\mathrm{Im}\{\chi^{(3)}\}}{f^4 c_{mol} N_A} \qquad (16)$$

where N_a is Avogadro's constant, C the concentration of the active species in the triplet state and f is Lorentz local field factor, $f = (\eta^2 + 2)/3$. Optimal values of γ are between 10^{-29}-10^{-34}.

The last parameter is the k term, and it is an indication of the ratio of triplet absorption cross section to singlet absorption cross section at a particular wavelength. This is important because in the case of phthalocyanines it is the triplet absorption which is most involved in optical limiting, as given in Equation 17 which gives an indication of how it's determined:

$$k = \sigma_{ex} / \sigma_g \qquad (17)$$

Also, the modified Jablonski diagram (Fig. 10) helps to describe where the two terms (σ_{ex} and σ_g) originate from. For any decent optical limiter this ratio needs to be above one, preferable quite a large amount above one.

Table 2 (and Figs. 11 and 12) list a selection of InPc derivatives that have been studied for their nonlinear optical behaviour [42, 44, 46, 49, 51].

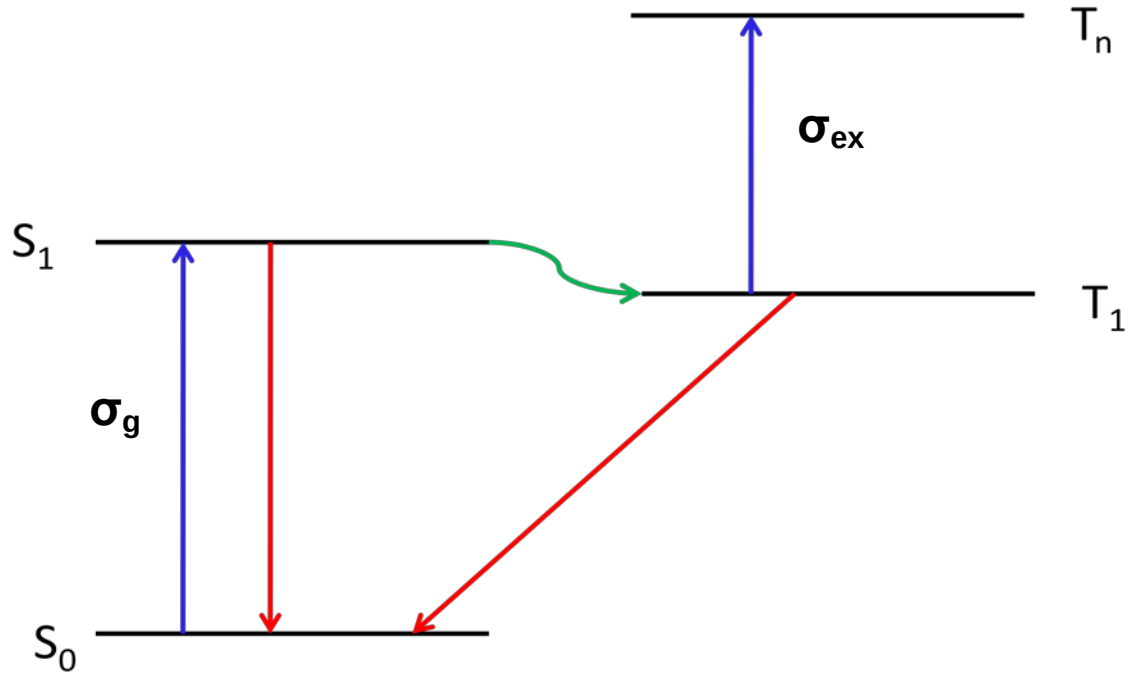

Fig. 10: Indication of the origins of the σ_g and σ_{ex} values.

Table 2: Nonlinear Optical Limiting Parameters for InPc Derivatives

Compound	**k**	**I_{lim}/J.cm^{-2}**	**Im[$\chi^{(3)}$]/10^{-11} esu**	**γ/10^{-32} esu**	**[Ref.]**
ClInPc			0.15		[46]
6a	16.1	10.1	1.2	7.3	[51]
6b	16.2	9.5	1.3	8.1	[51]
(tri-(n-hexyl)siloxy)InPc	16	0.24			[44]
7a		0.25			[42]
7b		0.09			[42]
7c		0.09			[42]
7d		0.66			[42]
7e	41.4	1.16	4.59	0.002	[49]

7f	53.4	1.92	2.87	0.00307	[49]
7g	9.44	1.47	6.81	0.00297	[49]

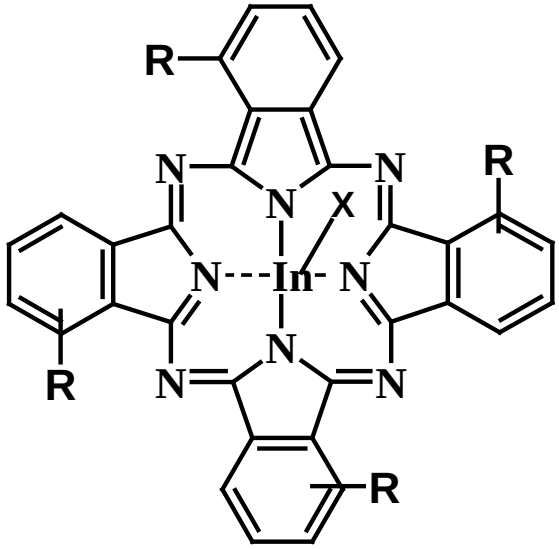

(6)

R = C_6H_5

X =Cl **a**

=ArF **b**

Fig. 11: Tetra Substituted InPc Derivatives 6a and 6b

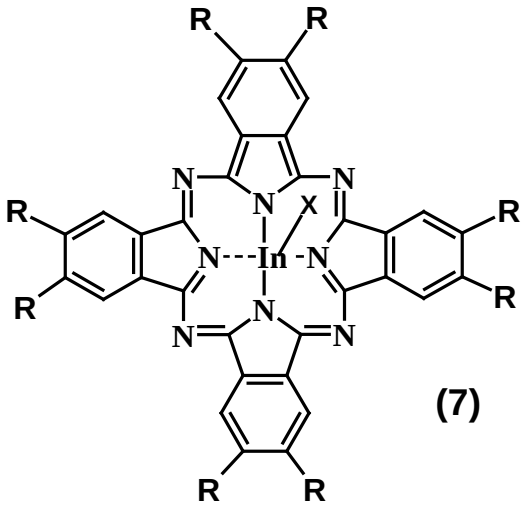

(7)

X = Cl, R_1 = H, R_2 = $-C(CH_3)_3$ **a**

X = Br, R_1 = H, R_2 = 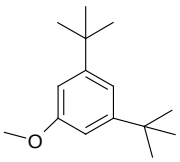 **b**

X = I, R_1 = H, R_2 = 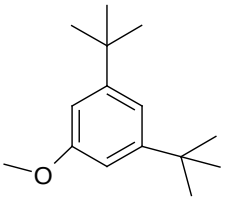 **c**

X = $OCOCF_3$, R_1 = R_2 = 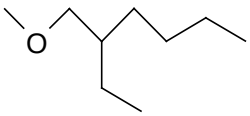 **d**

X = Cl, R_1 = R_2 = 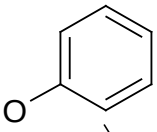 **e**

X = Cl, R_1 = R_2 = 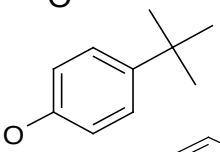 **f**

X = Cl, R_1 = R_2 = 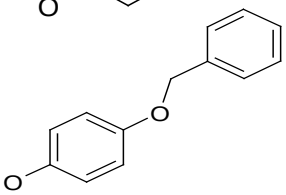 **g**

Fig. 12: Octa Substituted InPc Derivatives 7a-g.

As can be seen from Table 2, InPc derivatives (Figs. 11 and 12) have been fairly well examined as optical limiters. This work adds to the list of InPc derivatives used for nonlinear optics.

1.5 Summary of Aims

Studies involving QDs bound peripherally to Pcs is virtually non-existent. It therefore presents an interesting area of study due to the unknown properties that such a composite would possess. As has already been alluded to, any heavy compound bound to the conjugated ring system of the phthalocyanine tends to create an enhanced triplet-triplet absorption and QDs are generally made from heavy elements, so it stands to reason that QDs peripherally bound to a Pc should enhance the Pc's triplet quantum yield and consequently its photophysical behaviour.

Even if this is not the case, the incorporation of the properties of the QD and Pc into one molecule is beneficial because they complement one another. The QD's intense fluorescence can be used to bio-image the cancer cells that the conjugate will tend to localise in due to the nature of Pcs to be retained longer in cancer cells. The Pc may still possess its ability to produce singlet oxygen when part of a conjugate, meaning that whilst the conjugate is imaging the cancer cells it could also be destroying them. Lastly, depending on at which wavelength the QD emits, one may find FRET occurring between the QD and Pc. This is beneficial because it means that the Pc, which usually has very narrow areas of absorption, will effectively possess the QD's much broader absorption spectrum as well as its own. Thus it should be considerably easier to excite the Pc.

One last aspect that should be mentioned is that Pcs and QDs have been shown to possess optical limiting properties, thus a conjugate may enhance the optical limiting ability of one and/or the other, or it could just result in a cumulative effect of the optical limiting powers of the two.

To summarize objectives:

- To synthesize MTAPcs and link them to QDs
- To study the photophysics of MTAPc in the presence and absence of QDs (linked or mixed)
- To study the nonlinear optical limiting behaviour of the synthesized MTAPcs

Chapter 2

2. Experimental

2.1. Materials

N-hydroxysuccinimide (NHS) was obtained from Fluka. HCl and cadmium chloride were purchased from Merck. Mercaptoproprionic acid (MPA), 1,8-diazabicyclo[5.4.0] undec-7-ene (DBU), 1-chloronaphthalene (1-CNP), thioglycolic acid (TGA), tellurium powder, indium trichloride, 4-nitrophthalonitrile and N-(3-dimethylaminopropyl)-N'-ethylcarbodiimide hydrochloride (EDC) were from Sigma-Aldrich. Sodium borohydride, sulphuric acid, dimethylsulfoxide (DMSO), N,N'-dimethylformamide (DMF) and sodium hydroxide (NaOH) pellets were obtained from Saarchem. Urea was purchased from Riedel-de Haën. H_2Pc obtained from Aldrich and used as the standard for triplet quantum yield determination. The synthesis and characterization of ZnTAPc have been reported before [12].

2.2. Equipment

Fluorescence excitation and emission spectra were recorded on a Varian Eclipse spectrofluorimeter. UV-visible spectra were recorded on a Varian 500 UV-Vis/NIR spectrophotometer. ^{1}H Nuclear Magnetic Resonance (^{1}H NMR) spectra were obtained on a Bruker AMX 400MHz spectrometer. X-ray powder diffraction patterns were recorded on a Bruker D8, Discover equipped with a proportional counter, using Cu-Kα radiation (λ = 1.5405 Å, nickel filter). Data were collected in the range from 2θ = 5º to 60º, scanning at 1º min^{-1} with a filter time-constant of 2.5 s per step and a slit width of 6.0 mm. Samples were placed on a silicon wafer slide. The X-ray diffraction data were treated using the freely-available Eva (evaluation curve fitting) software. Baseline correction was performed on each diffraction pattern by

subtracting a spline fitted to the curved background and the full-width at half-maximum values used in this study were obtained from the fitted curves.

Triplet quantum yields were determined by recording the triplet absorption and decay kinetics from a laser flash photolysis system containing a Nd:YAG laser (Quanta-Ray, 1.5 J/ 90 ns), pumped tunable dye laser (Lambda Physic FL 3002, Pyridin 1 dye in methanol), a Thermo Oriel xenon arc lamp, a photomultiplier tube as a detector and a 3032C Tektronix 300MHz two-channel digital real-time oscilloscope (Fig. 13). Triplet lifetimes were determined using OriginPro 7.5 software. Infrared spectra were recorded using the Bruker Vertex 70, using potassium bromide (KBr) discs formed with the samples imbedded withing them, whilst the Raman spectra were obtained using a Bruker RAM III, using compacted sample to form a smaller disc which occasionally had KBr mixed into it.

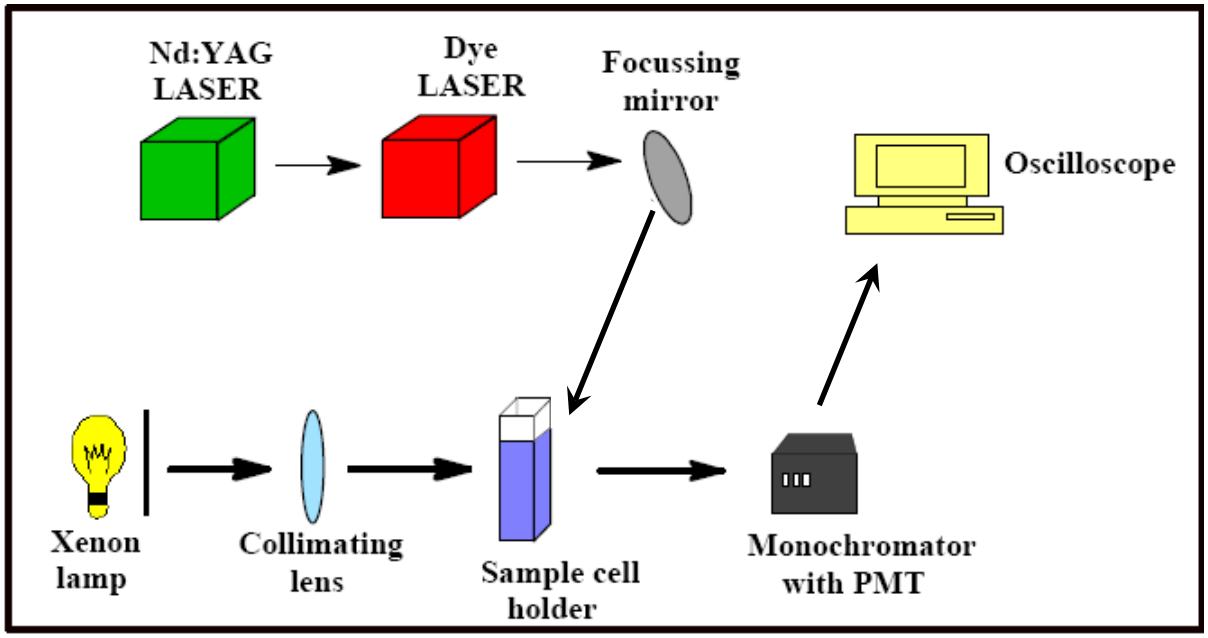

Fig. 13: Schematic Diagram of Laser Flash Photolysis Setup.

2.3 Synthesis of Pcs

2.3.1 Synthesis of 4-aminophthalonitrile, Scheme 3

4-nitrophthalonitrile was placed in a flask containing ethanol, palladium and activated carbon, and set to stir for 7 hrs under H_2. The resulting phthalonitrile was then purified of the palladium and carbon by filtering it through celite and the ethanol was evapourated off.

^{1}H NMR (DMSO-d_6): δ = 8.44 (1H, s, Ar-H), 7.75 (1H, s, Ar-H), 7.18 (1H, s, Ar-H).

2.3.2 Synthesis of indium tetraaminophthalocyanine (ClInTAPc), Scheme 3

ClInTAPc was synthesized according to methods reported for other MTAPc complexes [12], with slight modification, as follows: indium chloride (0.04g, 0.18mmol), 4-aminophthalonitrile (0.1g, 0.7mmol) and DBU (0.1ml) in 1-chloronaphthalene (10ml) were heated under reflux at 220^{o}C for 7 hr. The product was then washed (using a Soxhlet apparatus) with methanol, an aqueous HCl solution and acetone to remove impurities and starting materials.

Yield: 0.0221g, 17 %. Uv-Vis (DMF): λ_{max} nm (log ε) 374 (4.54), 711 (4.56); IR spectrum, KBr pellets (cm^{-1}): 3453.18 (N-H str.), 31294.17, 3059.56, 3025.36, 2852.14, 2533.11, 2361.17, 2343.29, 2230.38, 1770.24, 1722.41, 1657.80 (C=C str.), 1609.11 (N-H bend), 1525.21, 1481.31, 1435.21, 1386.15, 1335.74 (C-C str.), 1253.12 (C-C str.), 1140.36 (C-C str.), 1041.28 (C-N str.), 928.11, 905.15, 846.43, 745.61, 724.68, 697.34, 661.16, 523.59, 478.65. ^{1}H NMR (DMSO-d_6): δ = 8.30 (4H, s, Ar-H), 8.18 (d, 4H, Ar-H), 8.03 (4H, d, Ar-H).Calcd for $C_{32}H_{20}N_{12}ClIn$: C, 53.17; H, 2.76; N, 23.26 %. Found: C, 52.81; H, 3.42; N, 22.88 %.

2.4. Synthesis of CdTe QDs capped with mercapto propionic acid (MPA) or thioglycolic acid (TGA)

The preparation of an MPA or TGA capped QD was performed via a modified method adopted from literature [39, 52] (Fig. 14). Briefly, 2.35 mmol of $CdCl_2.H_20$ was dissolved in 125 ml of water and 5.7 mmol of the MPA or TGA stabilizer was added under stirring. The solution was adjusted to pH 11 by the dropwise addition of NaOH. Nitrogen gas was bubbled through the solution for about 1 hour, and this aqueous solution subsequently reacted with H_2Te gas. H_2Te gas was generated by the reaction of $NaBH_4$ with Te powder in the presence of 0.5 M H_2SO_4 under a flow of nitrogen gas. The solution was then refluxed under air at 100^oC for different times to control the size of the CdTe QDs. On cooling, the QDs were precipitated out of the solution using excess ethanol, and the solutions were then centrifuged to harvest the QDs.

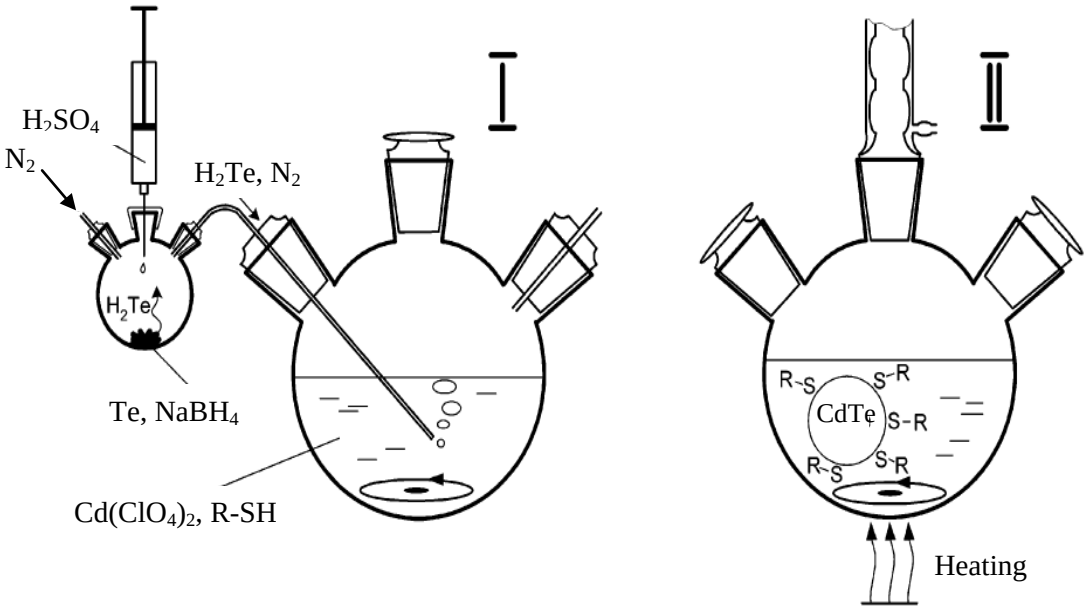

Fig. 14: Setup for synthesis of water-soluble CdTe Quantum Dots [29].

An alternate approach is the use of a sodium hydrogen telluride solution instead of hydrogen telluride gas. The formation of sodium hydrogen telluride is awkward because it, like many other steps in QD synthesis, is highly unstable in the presence of oxygen. Also, the reaction itself is heat sensitive as well, in that at high enough temperatures the reaction would occur too quickly to be controlled properly. For this reason, the reaction is carried out in a heavily de-aerated reaction system kept at 0^{o}C. The actual reaction only entails the stirring of tellurium powder and sodium borohydride in a small amount of deionised water, within the setup described above, for several hours until the grey tellurium powder becomes a clear solution with a white precipitate. The clear solution is the desired reactant, and can then be injected into the de-aerated cadmium solution. The advantage of using the solution over gas, is that a high concentration of telluride ions is guaranteed.

2.5 Synthesis of Pc Conjugates with QDs

For the formation of the linked QD-MTAPc, the mixture containing 2 mM NHS, 5 mM EDC, CdTe QDs (0.11 g/mL) and MTAPc (3.8×10^{-5} M) in pH 7.4 buffer was allowed to react for 1 h. NHS and EDC were used for the activation of the carboxylic acid group of the QDs, and the resulting linked complex is represented as QD-MTAPc. Experiments were also done where MTAPc were mixed with QDs without chemical linking, resulting in mixture, which is represented as QD:MTAPc. The linked QDs-ZnTAPc complex was purified of unlinked compounds by precipitating everything out with ethanol, which was afterwards evaporated off, then rinsed with water to remove the unlinked QDs and then THF to remove the unlinked ZnTAPc, thus ensuring that the effects of mixed QDs:ZnTAPc (not chemically linked) are eliminated. Ethanol was employed since none of the compounds dissolved in this solvent, whereas the QDs

were insoluble in THF and ZnTAPc was insoluble in water. The linked complex was insoluble in both THF and water. The remaining solid was redissolved in DMF:water 3:2.

2.6 Fluorescence Quenching studies

Fluorescence quenching studies were performed to check the quenching ability of MTAPc on QDs using a mixture of the two solutions. For the quenching studies of the QD's fluorescence by MTAPc, a solution of the 3 nm sized QD-TGA was titrated with varying concentrations (0 to 1.2 x 10^{-4} M) of the MTAPc derivatives in DMF: water (3:2). These mixtures represent mixed QD:MTAPc, and the solvent mixture employed was used in order to enable both MTAPc and the QDs to dissolve. In monitoring the QDs emission, the excitation wavelength used was at 550 nm and emission spectrum recorded between 560 and 800 nm. The steady decrease in the fluorescence intensity of QDs with an increase in the concentration of MTAPc complexes was related to MTAPc concentrations by equation 10 [41]. The number of binding sites on the QDs were determined using equation 11, for the mixed QD-MTAPc. Plots of $\log\left[\frac{(F_0-F)}{(F-F_\infty)}\right]$ against log [MTAPc] provided the values of n (binding sites, from slope) and k_b (binding constant, from the intercept).

2.7 Fluorescence Quantum Yields and FRET studies

Fluorescence quantum yields (Φ_F) of MTAPcs were determined by a comparative method [35] using equation 3. ZnPc in DMSO was used as a standard, Φ_F = 0.20 [36] for the determination of fluorescence quantum yields of the MPc derivatives in

3:2 DMF:water solvent mixture. The DMF:water 3:2 mixture had its refractive index determined with a refractometer. Rhodamine 6G in ethanol with Φ_F = 0.94 was employed as the standard for the determination of the fluorescence quantum yields of quantum dots [19, 37]. The determined fluorescence quantum yield values of the QDs were employed in determining their fluorescence quantum yields in the mixture with MTAPc derivatives ($\Phi_{F(QD)}^{Mix}$) or linked ($\Phi_{F(QD)}^{linked}$) using equations 4.

Once all of these fluorescence quantum yields are calculated, the FRET efficiency value can be determined using equation 9. Along with this, the spectral overlap and Förster distance of the Pc:QD combination (mixed or linked) is determined using PhotoChemCAD. Lastly, the calculated Förster distance and efficiency is used in equation 7 to determine the actual centre to centre distance between the Pc and QD.

Chapter 3

The results presented in this thesis have been published in journals listed below:

1 J. Britton, E. Antunes and T. Nyokong Fluorescence studies of quantum dots and zinc tetraamino phthalocyanine conjugates. **Inorg. Chem. Commun 12** (2009) 828-831

2. J. Britton, E. Antunes and T. Nyokong Fluorescence quenching and energy transfer in conjugates of quantum dots with zinc and indium tetraamino phthalocyanines. **J. Photochem. Photobiol. A. Chem**. in press

3. Results and discussion

3.1 Synthesis and Photophysical Characterization of MTAPc

3.1.1 Synthesis

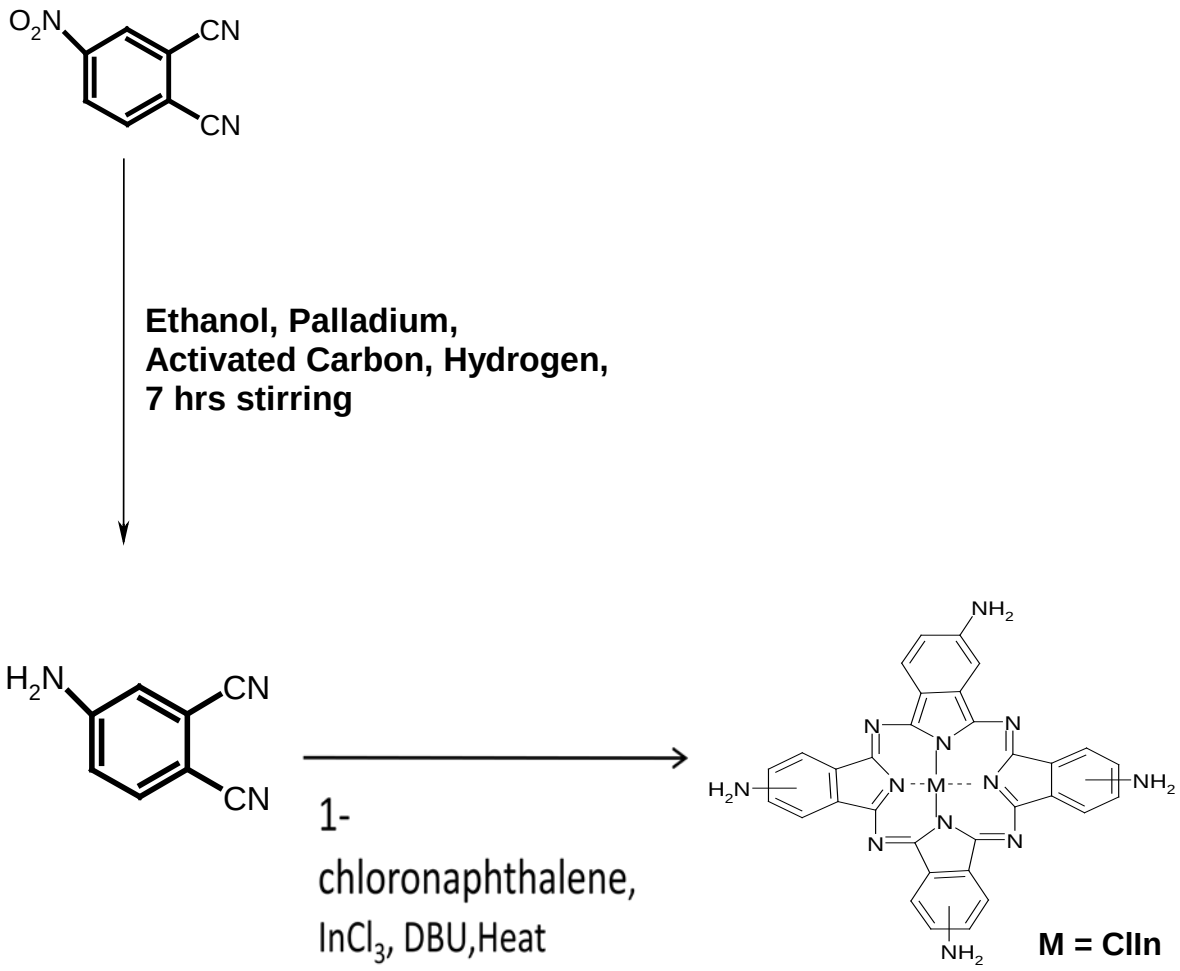

Scheme 3: Synthetic route for the creation of ClInTAPc

The ClInTAPc was synthesized from 4-aminophthalonitrile, instead of using the usual 4-nitrophthalonitrile and then converting the nitro groups to amino groups with ammonia [53], Scheme 3. Since $InCl_3$ was the metal salt of choice in the synthesis, 1-chloronaphthalene was used as the reaction solvent so that the high temperature

of 220^{o}C could be reached. A yield of 17% was obtained for the ClInTAPc. Fig. 15 is an infrared spectrum of the ClInTAPc with important bands indicated. NMR of ClInTAPc gave characteristic aromatic protons of a phthalocyanine between 8.0 and 9.0 ppm.

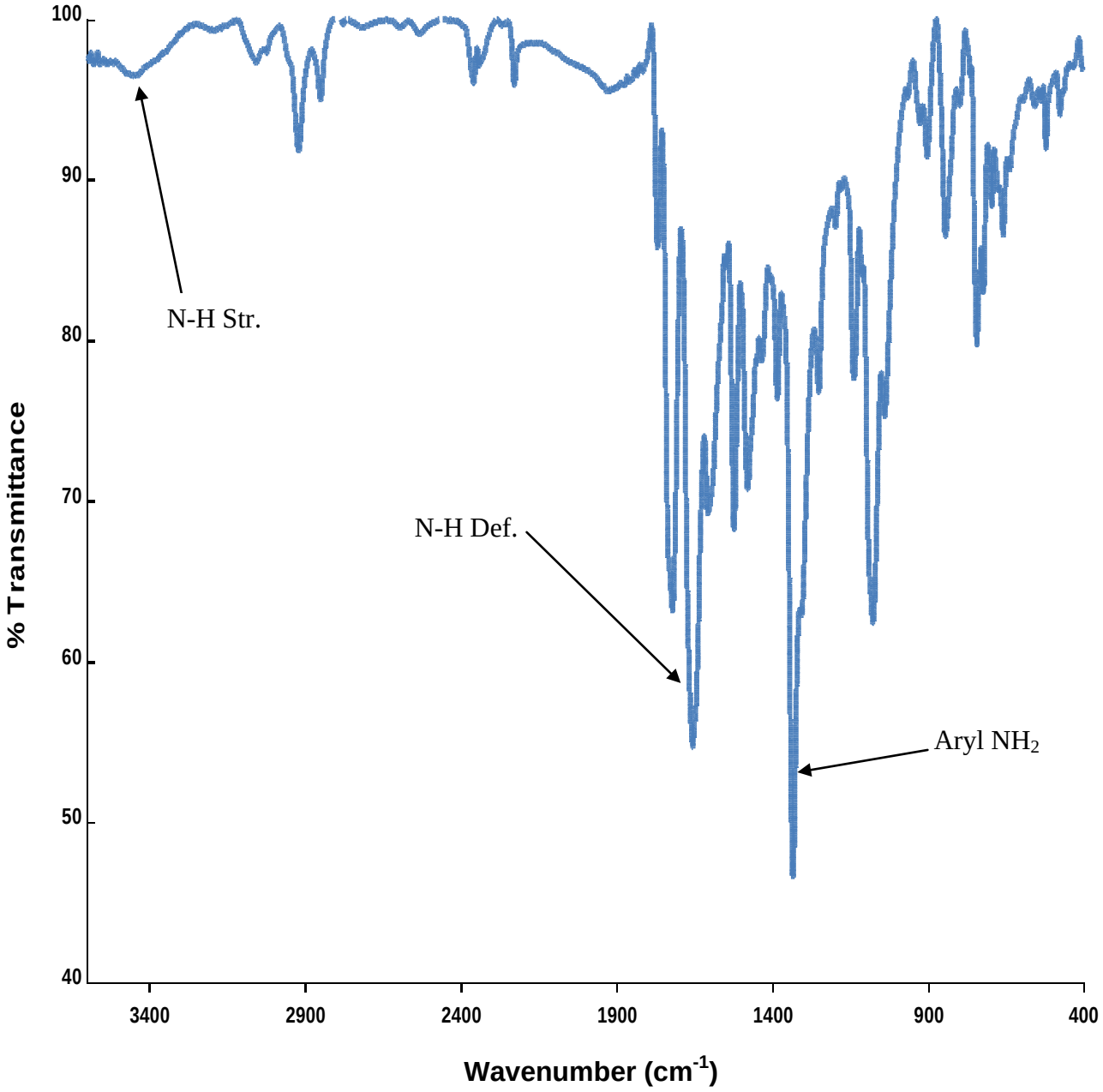

Fig. 15: Infrared Spectrum of InTAPc.

3.1.2 Absorbance and Emission spectra

Fig. 16(a) shows the UV-Vis spectrum of ZnTAPc, typical of amino phthalocyanine complexes, with a Q band at 702 nm in DMF. The red-shift in the spectrum compared to unsubstituted ZnPc (670 nm) is as a result of the electron-donating ability of the amino groups. Fig. 16(b) is the UV-Vis spectrum of InTAPc with a Q band at 713 nm in DMF. The InTAPc complex is more red shifted than ZnTAPc due to the electronic effects of the large central metal. Fig. 17 gives the absorption spectra of the two MTAPc list the UV-vis data in 1-chloronaphthalene and Table 3.

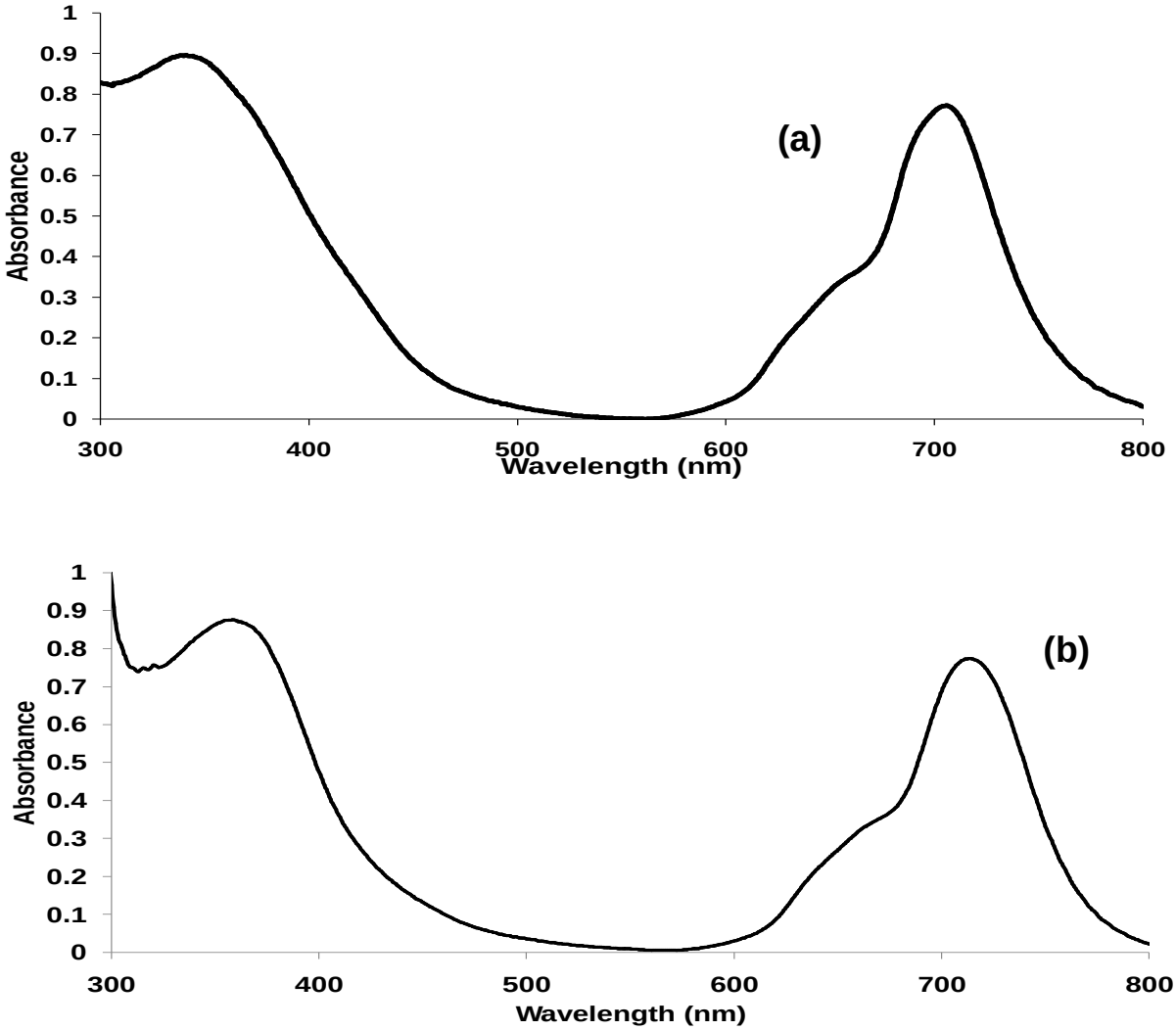

Fig.16: UV-Visible Spectrum of (a) ZnTAPc in DMF, Concentration ~ 1 x 10^{-6} M, and (b) InTAPc in DMF.

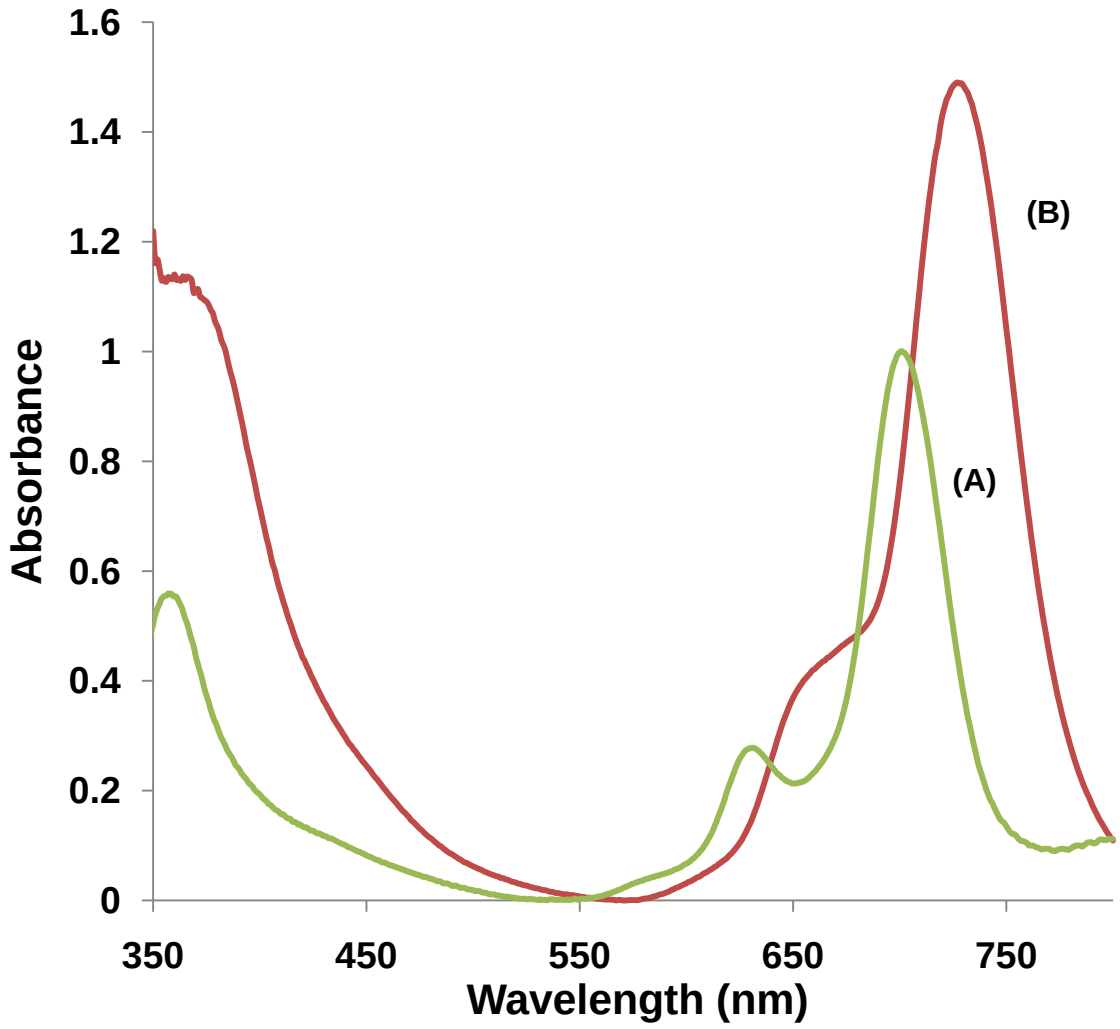

Fig. 17: Absorbance spectra of (A) ZnTAPc and (B) InTAPc in 1-chloronaphthalene.

Table 3: Photophysical Properties of Selected Phthalocyanines.

Compound	Absorption	Emission	Φ_F	Φ_T	τ_T (μs)
ZnTAPc	706[a] (704)[b]	723[a]	0.0033[a]	0.47[b]	4.96[b]
InTAPc	710[a] (724)[b]	-[c]	-[c]	0.71[b]	9.96[b]

[a] = values in DMF:water 3:2 (in solvent mixture since it will be used for FRET studies)

[b] = values in 1-CNP

[c] = too weak to be accurately determined

The shift to longer a wavelength in 1-chloronaphthalene for ClInTAPc could be due to either the destabilization of the highest occupied molecular orbital (HOMO) or the stabilization of the lowest unoccupied molecular orbital (LUMO). It has been suggested that the interaction between coordinating solvents and the phthalocyanine molecule, stabilises the LUMO of the complexes. The observed red shift suggests that 1-chloronaphthalene containing an extend π system stabilizes the LUMO. It is known that the Q band shifts to longer wavelengths with enlargement of π conjugated system of the phthalocyanine ring [54]. Also, interactions between the chlorine atoms of the solvent and ClInTAPc could affect the Q band position, something which would not arise with ZnTAPc because it has no chlorine atoms in its structure.

The emission spectrum was a mirror image of the absorption spectrum for ZnTAPc, with its emission wavelength being given in Table 3. For InTAPc the emission peak was too weak to be accurately determined due to the heavy atom effect which encourages intersystem crossing to the triplet state.

3.1.3 Triplet Quantum Yields and Lifetimes, and Fluorescence Quantum Yields

The fluorescence quantum yields were determined with equation 3 using ZnPc in DMF as a standard. Both the refractive indices of DMF and the DMF:water mixture were determined for the calculation. The triplet quantum yields were determined with equation 5 using H_2Pc in 1-chloronaphthalene as a standard.

Fig. 18A shows the differential transient curve and the triplet decay curve for ClInTAPc in DMF. Similar curves were obtained for ZnTAPc. The triplet-triplet absorption maximum is observed at 525 nm, typical of most MPcs [39]. The singlet depletion curve is similar to the absorption curve. Fig. 18B also shows the triplet decay curve for the ClInTAPc obeyed second order kinetics. This is typical of MPc complexes at high concentrations (> 1 x 10^{-5} M) [55] due to triplet-triplet recombination. The concentrations employed in this work were in this range hence triplet-triplet recombination is expected.

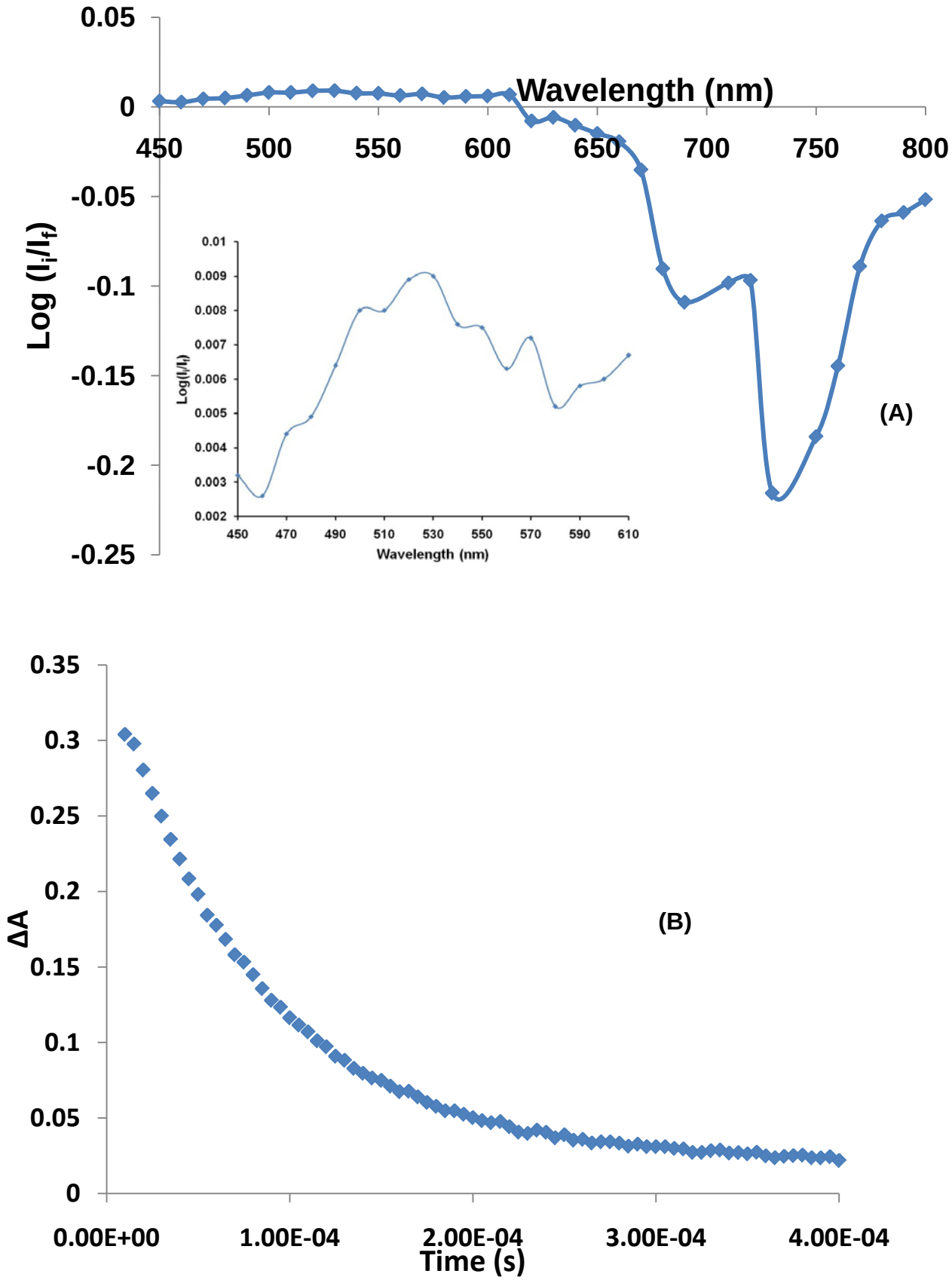

Fig. 18: (A) Differential Transient Curve for ClInTAPc in DMF and (B) Triplet Decay Curve of ClInTAPc in DMF.

The low Φ_F for ZnTAPc in Table 3 is probably due to fluorescence quenching by amino groups.

Table 3 gives the calculated triplet quantum yields and lifetimes (calculated using data from Fig. 18) of the ZnTAPc and InTAPc. As expected, the InTAPc had the higher triplet quantum yield due to the heavy atom effect on indium, which enhances intersystem crossing of the molecule to the triplet state. It is unclear as to why the lifetimes are so low, especially for the ZnTAPc, which contains the smaller central metal and should have a value closer to the 350μs of ZnPc [39]. The values for the InTAPc seem more realistic because the heavy atom effect generally causes low lifetimes. A plausible explanation for the ZnTAPc is that the amino groups are perhaps quenching the triplet state of the molecule, resulting in a short lifetime.

3.1.4 Nonlinear Optical Parameters

Table 4: Calculated Photophysical and Optical limiting parameters of ZnTAPc and InTAPc in 1-chloronaphthalene. See Fig. 12 for complex numbering.

Compound	**k**	**Im[$\chi^{(3)}$]/10^{17}**	**$\gamma/10^{37}$**	**Ref.**
ZnTAPc	6.0[a]	0.9[a]	0.5[a]	-
InTAPc	1.8[a]	8[a]	1.2[a]	-
7e	41.4[b]	4590000[b]	200[b]	[49]
7f	53.4[b]	2870000[b]	307[b]	[49]
7g	9.44[b]	6810000[b]	297[b]	[49]

[a] = 1-chloronapthalene

[b] = DMSO

Table 4 lists the calculated optical limiting parameters of I_{lim}, k, third-order susceptibility and hyperpolarizability for ZnTAPc and InTAPc. The k value, equation 17, was above one indicating that the absorbance around the 532 nm region will predominantly be triplet-triplet absorption (Fig. 19), however the value is rather on the low side which will probably mean that the triplet-triplet absorption won't be as strong or pronounced as it should be, when compared to literature. I_{lim} values were unreasonably low and hence not shown in Table 4.

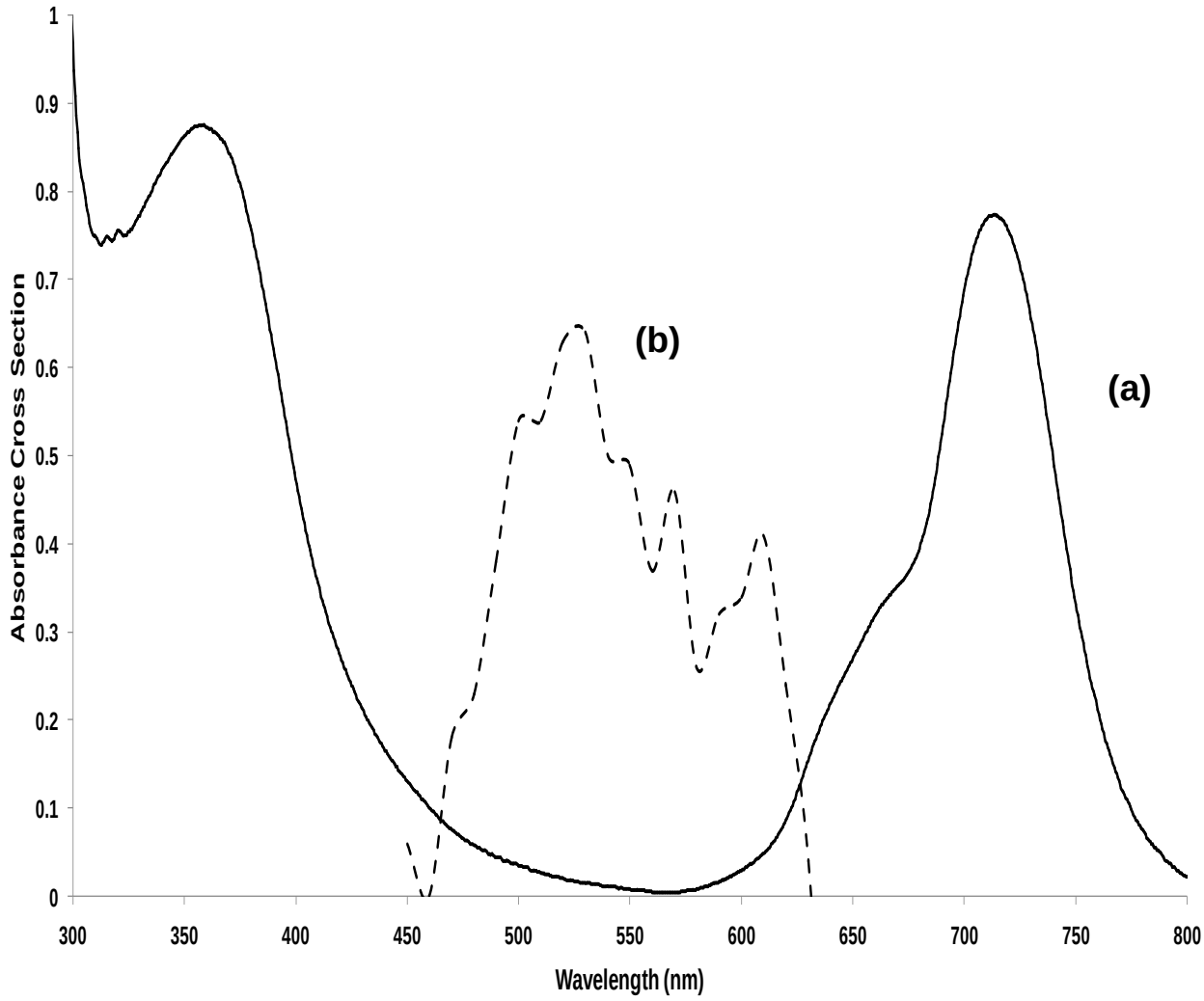

Fig. 19: Shows the normalized overlapped absorption spectrum (a) and differential transient curve data (b) of InTAPc, indicating mainly triplet-triplet absorption occurring at 525 nm.

Optimal values for Im[$\chi^{(3)}$] (equation 13) range from between 10^{-9} – 10^{-11} [49], and as is seen from Table 6 the calculated results fall below this range at the 10^{-17} region. This was also proved to be the case with the hyperpolarizability (γ) values (equation 16) which ranged between 10^{-37} – 10^{-38}, well below the optimal 10^{-29} – 10^{-34} range. Taking the parameters in their entirety, it seems that the two MTAPc analyzed are not particularly useful optical limiters, however the InTAPc is the better of the two

due to the heavy atom effect which enhances intersystem crossing and consequently triplet quantum yield.

3.2 Characterization of QDs

The X-ray diffraction pattern of the TGA capped CdTe QDs in solid nanocrystal form was employed in this work is shown in Fig. 20. The diffraction pattern shows three characteristic peaks for bulk CdTe structure. Size determinations using the XRD peak at $2\theta = 24$ (Fig. 20), were found to range between 3.0 nm and 3.4 nm (Table 5), hence in the same range as those determined by the polynomial fit from the UV spectrum, Table 5. For further studies CdTe-TGA QDs of 3.0 nm size and CdTe-MPA QDs of 3.5 nm and 3.0 nm sizes were employed (sizes from polynomial fit).

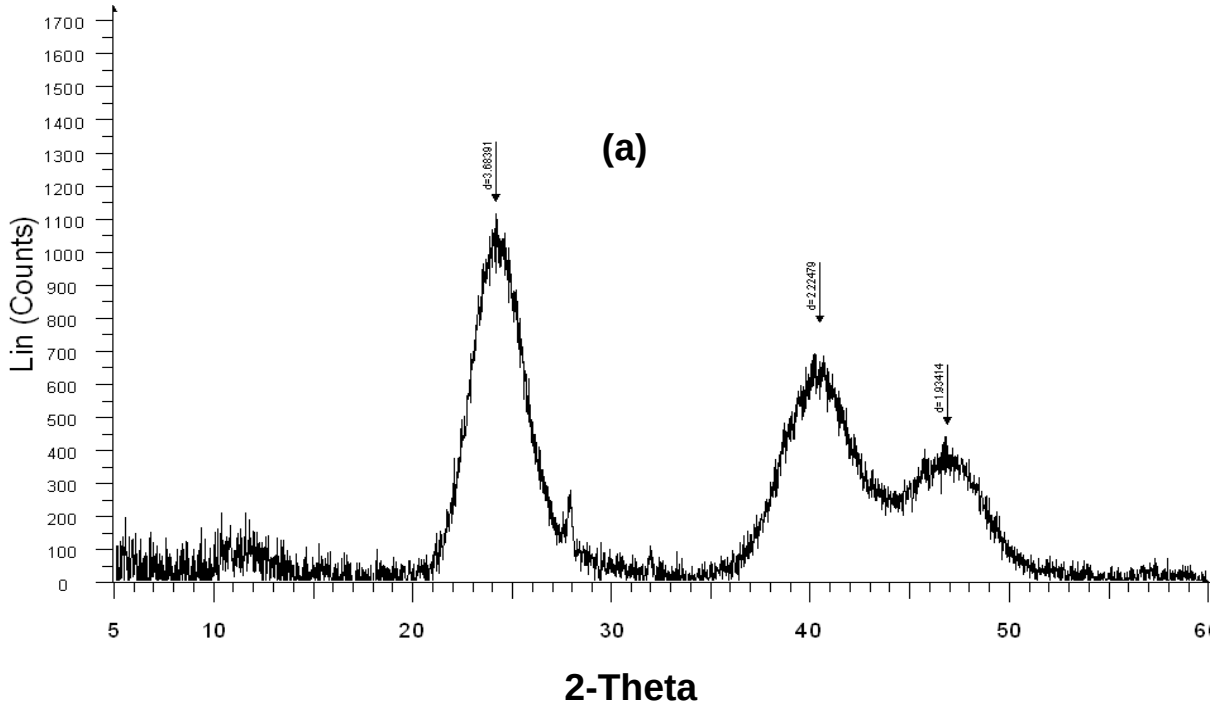

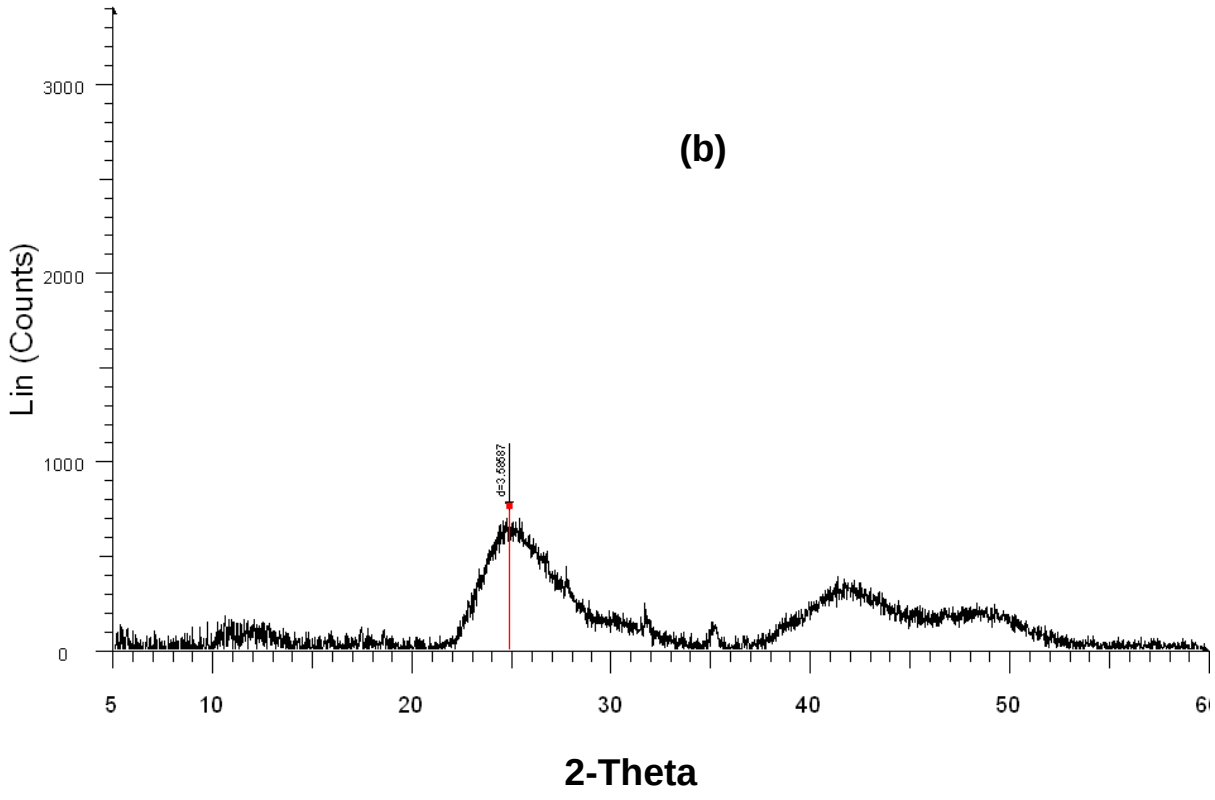

Fig. 20: XRD plot for (a) CdTe-TGA solid and (b) CdTe-MPA solid.

Table 5: Size Determination and Fluorescence Data for Synthesized CdTe QDs, the latter in DMF:water 3:2.

QD	Emision (nm)	Polynomial Size (nm)	XRD Size (nm)	Φ_{FQD}
MPA 1	597	3.5	3.0	0.047
MPA 2	566	3.0	-[a]	0.163
TGA	565	3.0	3.4	0.070

[a] = not determined

QDs grow through the Ostwald ripening process during the course of heating. As they grow, both the absorbance and the emission spectra shift to longer wavelengths. The MPA capped CdTe QDs displayed their first emission peak at 512 nm after 30 min of refluxing and were grown until their emission peak reached a maximum of 746 nm, indicating different sizes, Fig. 21. The TGA capped CdTe were grown to 3.0 nm (polynomial fit).

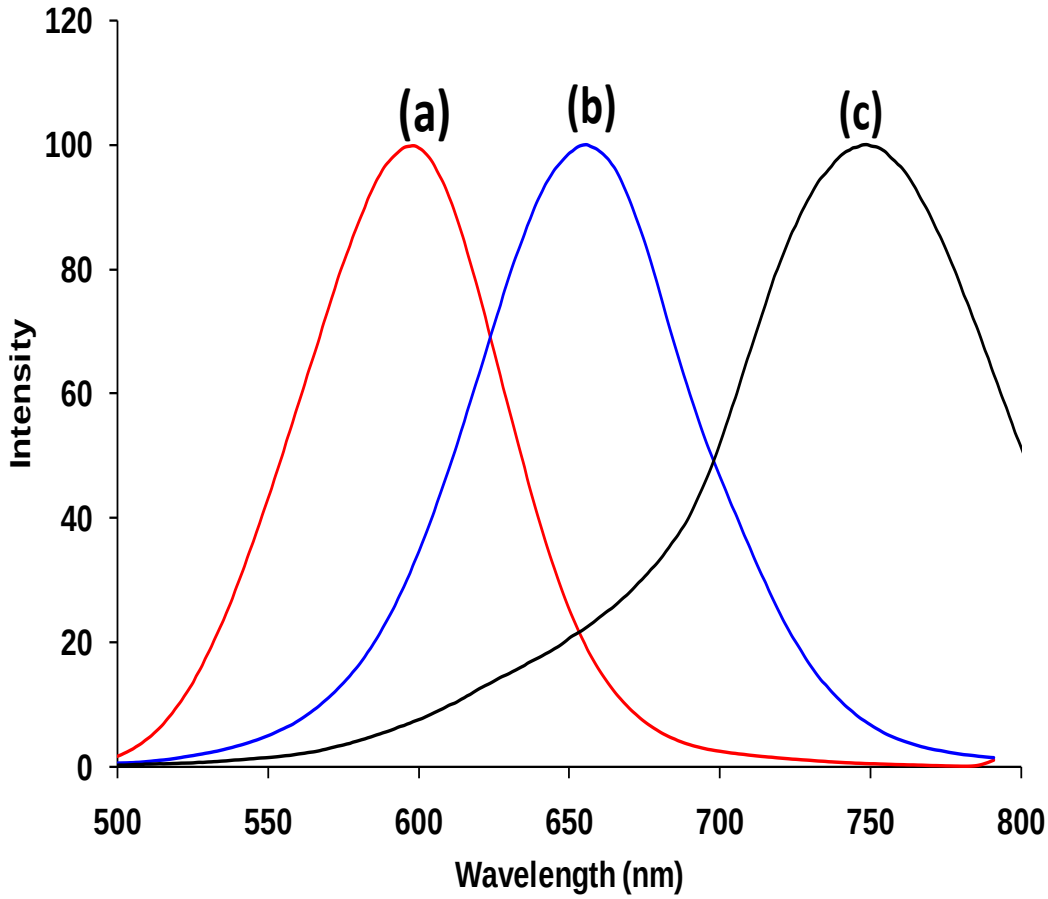

Fig. 21: Emission spectra of different sizes of MPA QDs (a) 3.0 nm, (b) 3.5 nm and (c) 4.1 nm in pH 11 buffer. Excitation = 400 nm.

Fig. 22 overlays the absorption and emission spectra of the CdTe – MPA QDs. The absorption spectra are broad, whereas the emission spectra display narrow well-defined peaks with a full width at half maximum (FWHM) around 60 nm, as typically obtained for certain QDs [56]. As is observed, there is a decrease in Φ_{FQD} values with increase in the size of QDs, Table 5.

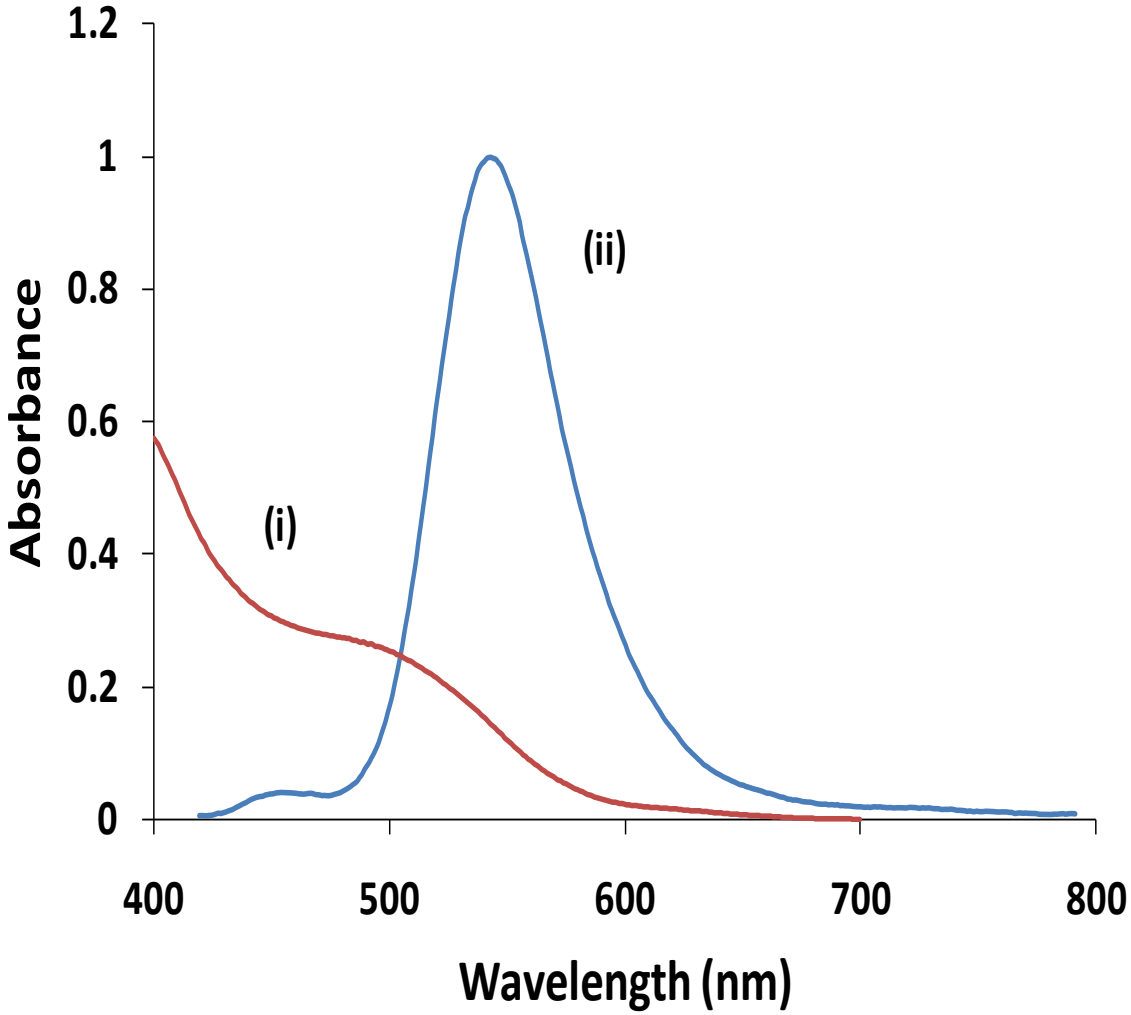

Fig. 22: Absorption (i) and emission (ii) spectra of CdTe QDs (MPA capped). Solvent = pH 11 buffer. Size of QDs = 3.0 nm. Excitation = 400 nm.

3.3 Formation of QD-MTAPc Conjugates

CdTe QDs were mixed with MTAPc, in the absence of EDC/NHS (represented as mixed QD:ZnTAPc, where QD represents CdTe-MPA or TGA capped QDs, as well as linked with MTAPc using ECD/NHS (represented as linked QD-ZnTAPc). For the mixed QD:ZnTAPc, the mode of interaction is thought to be most likely due to adsorption. The UV/visible spectra (Fig. 23) showed that there is only a 2 nm shift of

the Q band from 706 nm (for ZnTAPc alone or mixed QD-ZnTAPc in DMF:water) to 704 nm for linked QD-ZnTAPc. The reason for the shift is that the linkage has increased the HOMO-LUMO gap of the Pc involved, due to change in environment. The shift occurred with both TGA and MPA capped QDs.

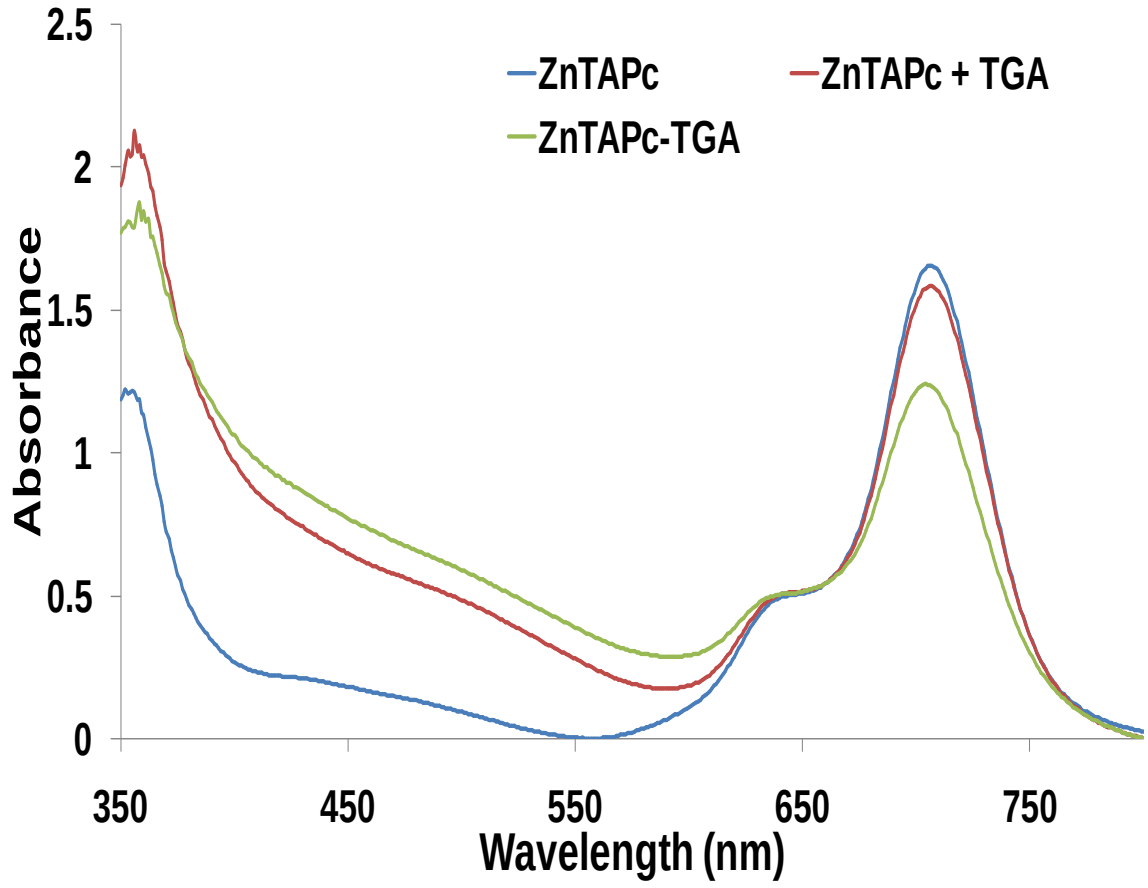

Fig. 23: Electronic absorption spectra of ZnTAPc (blue), ZnTAPc + CdTe-TGA (mixed) (red), and ZnTAPc+ CdTe-TGA (linked) (green) in DMF:water 3:2.

With the linked QD-MTAPc, the capping agent located on the surface of CdTe QDs were linked to MTAPc by coupling of the carboxylic group of the capping agent with the amine group on MTAPc, EDC/NHS mixture was used to activate the carboxylic acid group of the capping agent of the QDs to facilitate linking with the amine group of MTAPc, Scheme 4.

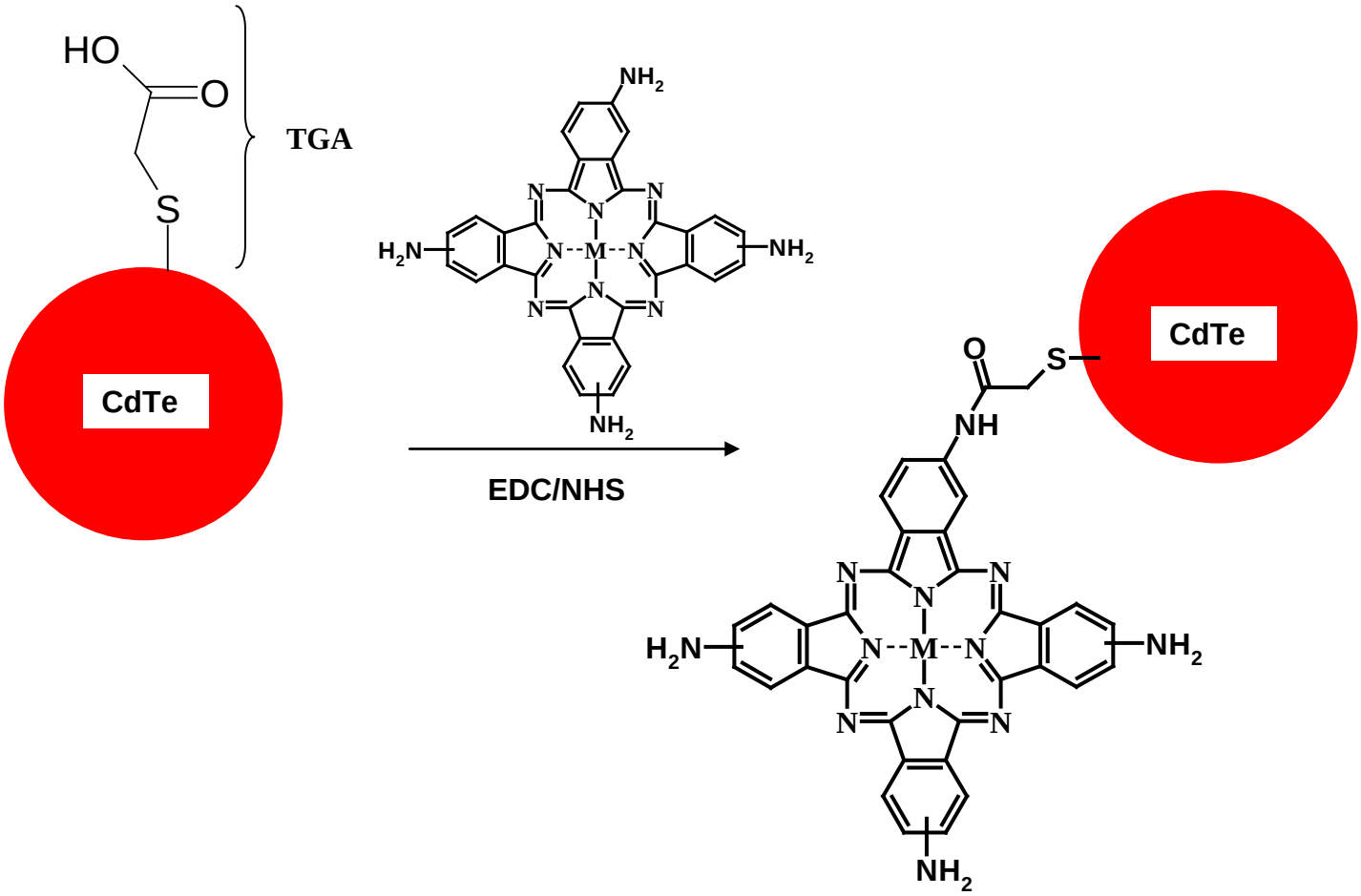

Scheme 4: Linking of CdTe-TGA to MTAPc using EDC/NHS as coupling agents.

However, it is possible for more than one amino group of the MTAPc to be linked to the QDs. The linked QDs-ZnTAPc complex was purified of unlinked compounds by precipitating everything out with ethanol, which was afterwards evaporated off, then rinsed with water to remove the unlinked QDs and then THF to remove the unlinked ZnTAPc, thus ensuring that the effects of mixed QDs:ZnTAPc (not chemically linked) are eliminated. Ethanol was employed since none of the compounds dissolved in this solvent, whereas the QDs were insoluble in THF and ZnTAPc was insoluble in water. The linked complex was insoluble in both THF and water. The remaining solid was redissolved in DMF:water 3:2. The proof for the formation of the amide bond was provided for linked ZnTAPc-CdTe-MPA, using infrared (IR) and Raman spectroscopy

(Fig. 24 and Fig. 25.), with the TGA capped QDs creating similar Raman and IR spectra.

The main element of the IR spectrum that proves the formation of the amide link is the reduction in intensity or disappearance of the aryl NH_2 signals, which can only happen if the amide link had formed. The fact that the signals 1500 cm^{-1} and 3200 cm^{-1} are altered between the mixed and linked solutions also gives indication of a structural alteration. In the linked QD-ZnTAPc form, there was an indication of an amide bond with the band at 3400 cm^{-1} (ν_{NH} (CONH)), while the ZnTAPc alone showed a broad band around 3300 cm^{-1}. Characteristic amide band was also observed at about 1654 cm^{-1} in the linked and not really in the ZnTAPc alone.

The Raman spectra is a complimentary technique to IR, and in this particular case the disappearance of the signals also indicated a structural change between the mixed and linked solution which can only be accounted for by the formation of the amide link. What was observed as predominantly different between the mixed QD:ZnTAPc and the linked QD-ZnTAPc was the absence of the peaks between 3000 and 3300 cm^{-1}, attributed to the QD structure, and absence/reduction of the peaks around 1500 cm^{-1}, attributed to the ZnTAPc structure, in the linked QD-ZnTAPc Raman spectrum, whereas these peaks were present in the mixed QD:ZnTAPc Raman spectrum.

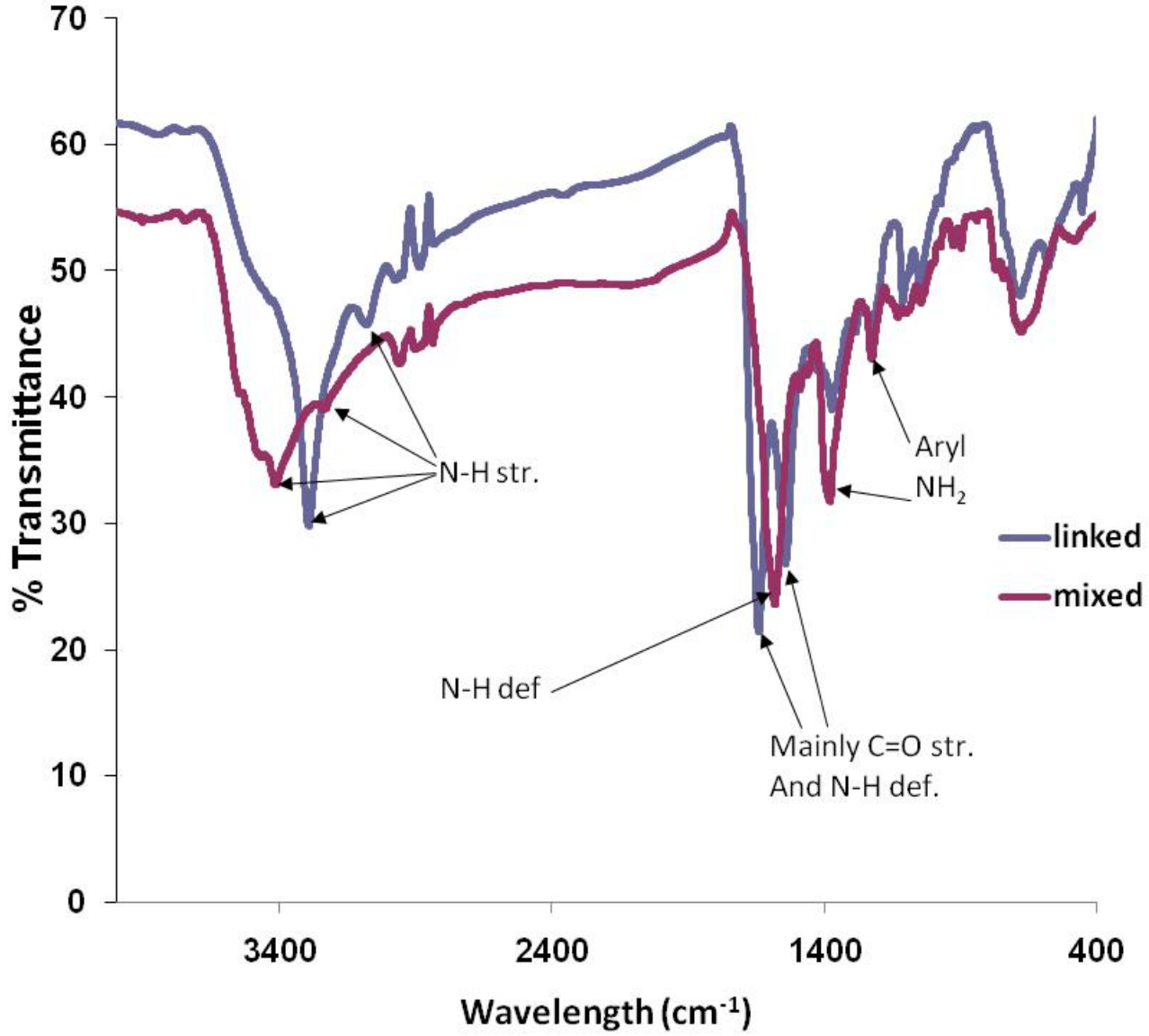

Fig. 24: Infrared Spectra of the CdTe-ZnTAPc mixture and linked complex.

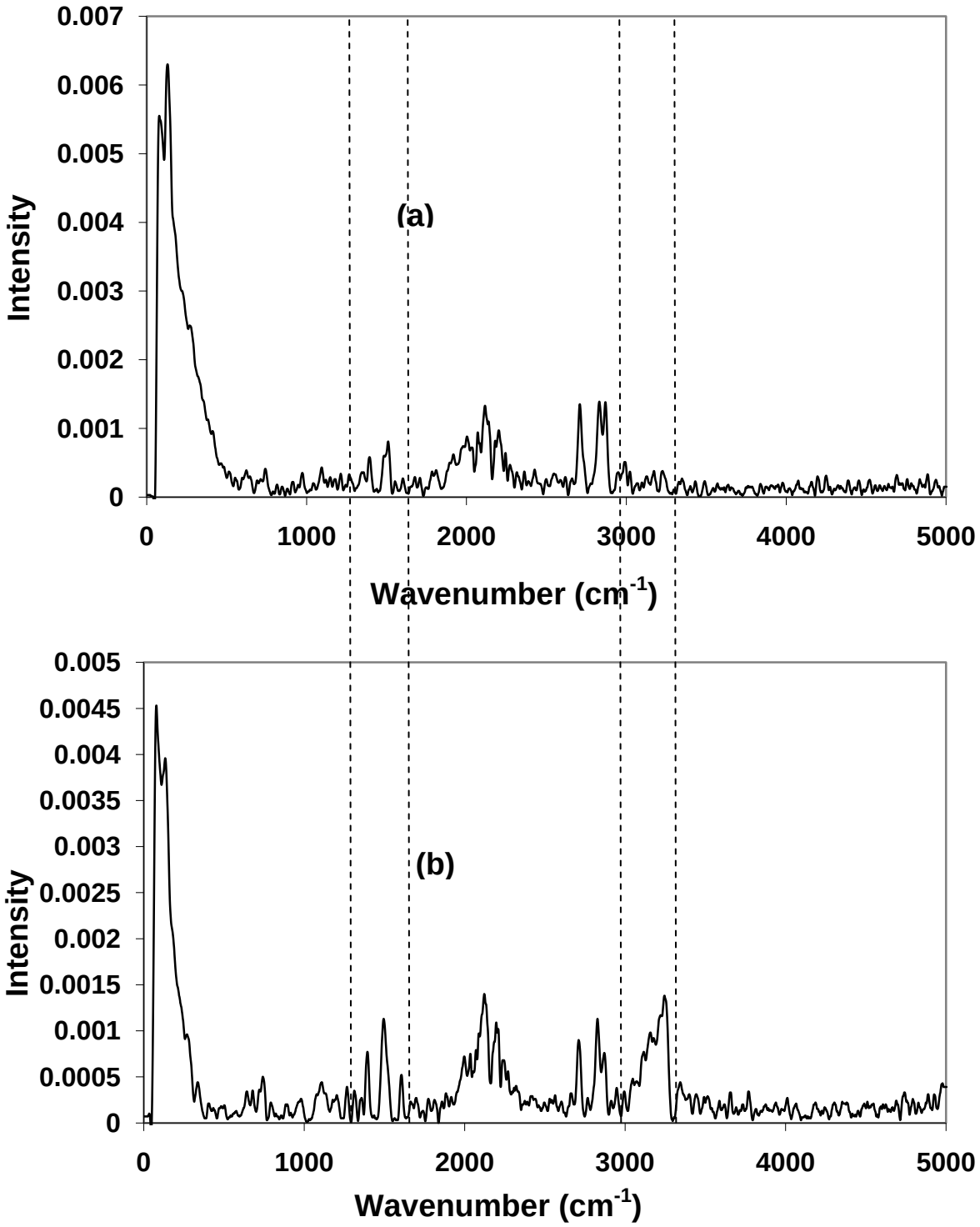

Fig. 25: Raman Spectra of (a) CdTe-ZnTAPc linked and (b) CdTe+ZnTAPc mixed

3.4. FRET studies

Förster resonance energy transfer (FRET) is a nonradiative energy transfer from a photoexcited donor fluorophore, after absorption of a higher energy photon, to an acceptor fluorophore of a different species which is in close proximity. The occurrence of FRET is made evident by a decrease of the donor photoemission accompanied by an increase in the acceptor's fluorescence. In order for FRET to occur, there has to be an overlap between the emission of the QDs and the absorption of the MTAPc, as seen in Fig. 26.

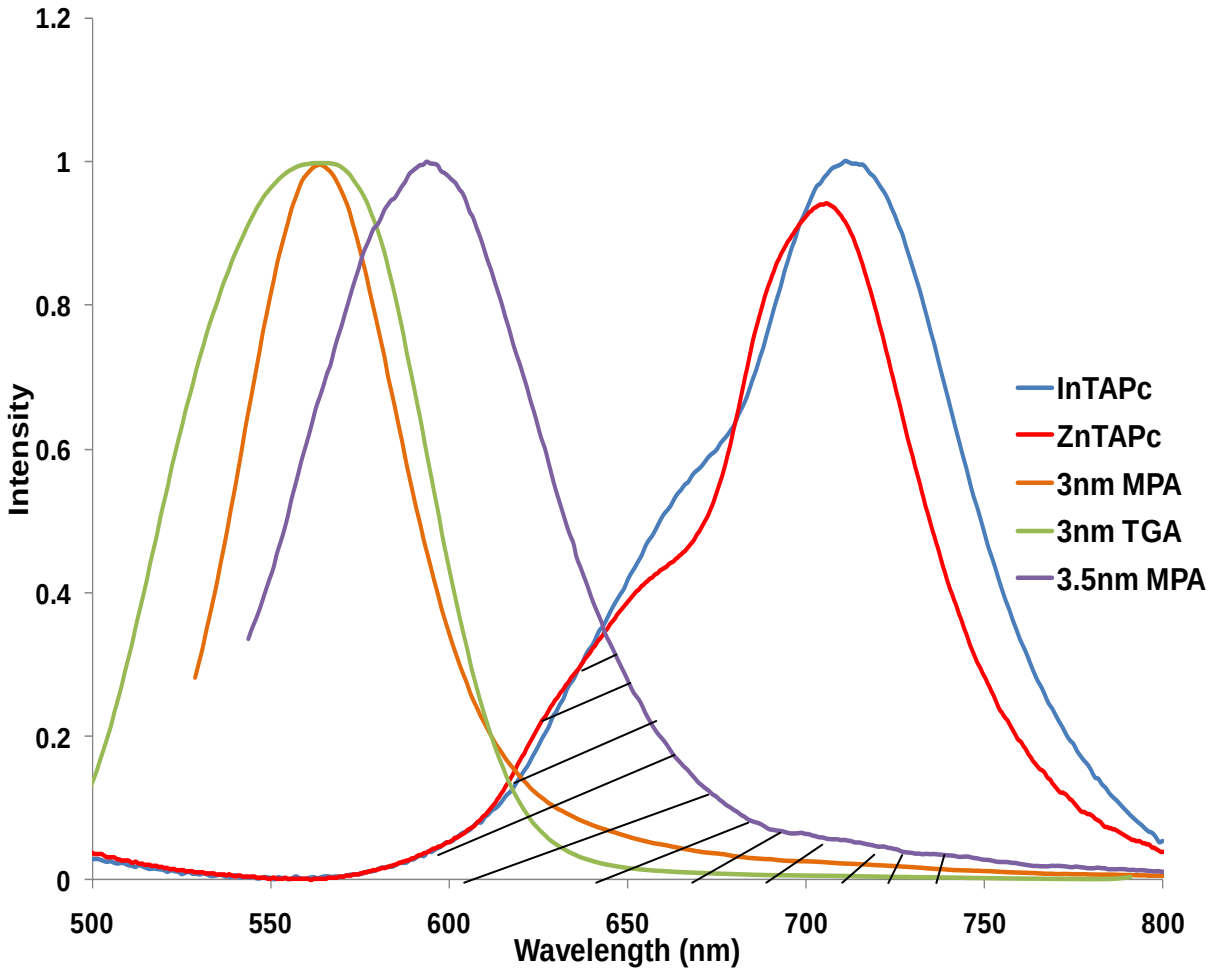

Fig. 26: Absorbance Spectra of ZnTAPc and InTAPc in DMF overlayed with the emission spectra of 3 nm and 3.5 nm MPA capped CdTe and 3nm TGA capped CdTe in DMF:water 3:2.

For the linked QD-MTAPc complex excitation was carried out at 550 nm where QDs absorb and MTAPc (in 3:2 DMF: water) does not. Weak fluorescence was observed around 750 nm for the MTAPc alone upon excitation at 550 nm, Fig. 27A(a) and B(a). The reason for the shift in the ZnTAPc emission peak to the red is not fully understood but probably has something to do with the solvent system decreasing the HOMO-LUMO gap of the Pc. A clear emission peak, however, was observed for the for ZnTAPc in the QDs:ZnTAPc (linked or mixed), Fig. 27A, upon excitation at this same wavelength, suggesting transfer of energy, through FRET, from the CdTe-TGA QDs to ZnTAPc. Thus this observation of ZnTAPc emission in the presence of QDs, confirms energy transfer from QDs to ZnTAPc. The stimulated emission observed for the linked (QD-ZnTAPc), Fig. 27A, is however, weaker than that for the mixture (QD:ZnTAPc), though the relative amounts of ZnTAPc and QDs will be different in the mixed and linked QD-ZnTAPc, making comparison difficult. There is no definitive answer as to why the stimulated emission of the linked compound is less than the mixture, however it probably has to do with internal conversions occurring within the linked compound that is dissipating the transferred energy, and only a fraction of it is being emitted by the phthalocyanine portion of the compound.

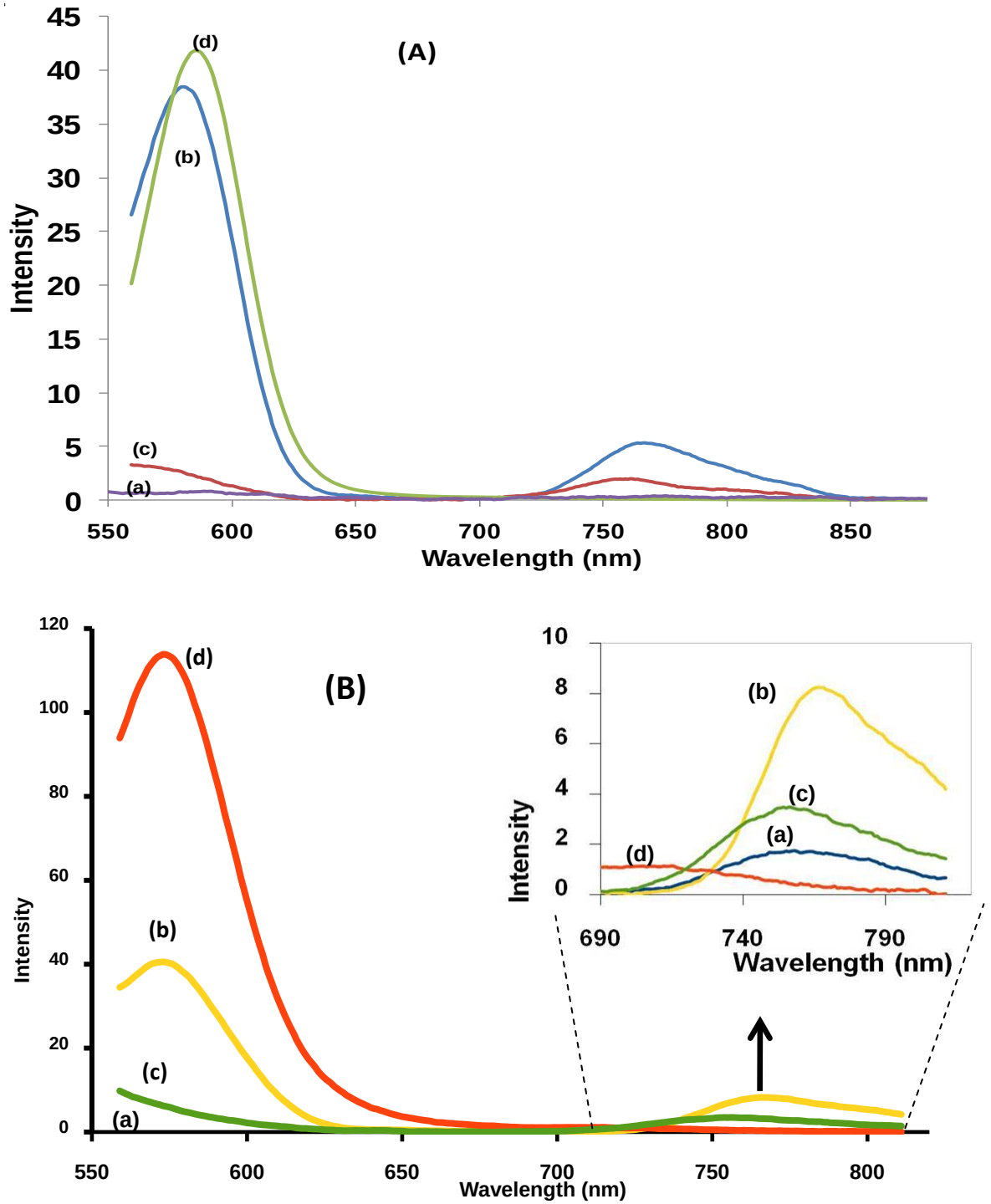

Fig. 27: Emission Spectra of (a) ZnTAPc alone, (b) mixed QD-ZnTAPc, (c) linked QD-ZnTAPc and (d) QDs alone. (A) TGA capped QDs and (B) MPA capped QDs.

Excitation at 550 nm in DMF:water 3:2. Size = 3 nm. Inset: Expanded area showing stimulated emission of ZnTAPc.

No FRET was observed for InTAPc (mixed or linked) in the presence of QDs (MPA or TGA capped), most probably due to the heavy atom present in InTAPc. A heavy atom such as indium would result in a low fluorescence emission, as most energy in the excited singlet state undergoes intersystem crossing to the triplet state. However, ClInPc does quench quantum dots emission, as discussed below.

The efficiency of energy transfer between QDs and MTAPc (Eff) was calculated using $\Phi_{F(QD)}$ and $\Phi^{Mix}_{F(QD)}$ (and equation 8) Table 6. Eff is known to be dependent on a number of parameters such as the spectral overlap term (J, equation 6) estimated by overlapping QD emission with the absorbance of MTAPc derivatives shown in Fig. 26. This extent of overlap has varied units and in this work the units used were in cm^6 [19]. The PhotochemCAD program gives J units as cm^6 following the use of ε_{MTAPc} in $M^{-1}cm^{-1}$ and the wavelength λ in nm in equation 6. The Förster distance, R_0 (Å), equation 9, is the critical distance between the donor and the acceptor molecule fluorophores for which efficiency of energy transfer is 50% [57,58], and the center-to-center separation distance is between donor and acceptor chromophores (r, Å). The J and R_0 values in this work were computed using PhotochemCAD [39] while the r values were calculated using equation 7. All values are listed in Table 6.

Table 6: Energy transfer parameters for MTAPc in the presence of QDs. Size of QDs: CdTe-MPA = 3.5 nm and 3.0nm, CdTe-TGA = 3.0 nm. Solvent = DMF:water (3:2).

QD size (nm)	Complex	J /10^{14} cm^6 K	R_0 /10^{10} m	r /10^{10}m	*Eff*
3.0	ZnTAPc + MPA mixed [24]	3.43	30.8	25.9	0.74
3.0	ZnTAPc-MPA linked	3.43	30.8	20.0	0.93
3.0	ZnTAPc + TGA mixed	2.18	24.8	22.0	0.68
3.0	ZnTAPc-TGA linked	2.18	24.8	21.6	0.70
3.0	ClInTAPc + MPA mixed	1.02	25.1	22.2	0.69
3.0	ClInTAPc-MPA linked	1.02	25.1	17.0	0.92
3.0	ClInTAPc + TGA mixed	0.640	20.2	17.0	0.74
3.0	ClInTAPc-TGA linked	0.640	20.2	11.5	0.97
3.5	ZnTAPc + MPA mixed	8.90	29.3	39.2	0.16
3.5	ZnTAPc-MPA linked	8.90	29.3	26.6	0.65
3.5	ClInTAPc + MPA mixed	3.0	24.5	21.2	0.71
3.5	ClInTAPc-MPA linked	3.0	24.5	15.8	0.93

J values are generally of the order 10^{-14} cm^6 for porphyrin based molecules [57] and the values obtained in this work were of this order (in general) for the overlap between the QDs and MTAPc, Table 6. As expected, the J values were larger for the larger QDs. r values were smaller than R_0 values indicating that the Eff will be greater than 50% as observed. This applies for all MTAPc-QD combinations with the exception of ZnTAPc plus CdTe-MPA (3.5 nm), where r is larger than R_0, and hence

Eff is less than 50%. The FRET efficiencies reported in this work are higher than reported in the literature [21], see also Table 1, for other MPc complexes, using the same QDs. The evidence of a high FRET efficiency is also evident in Fig. 27 for ZnTAPc where there is a fast decrease in QDs emission on addition of the Pc to the QD. For ClInTAPc, FRET was not observed due to the heavy atom effect of In. In all cases, higher Eff values were observed for the linked complexes compared to the mixed QDs-MTAPc combinations, showing the advantages of chemical linking. However, as Fig. 27 shows, less FRET was obtained for the linked than for the mixed complexes, suggesting that even though there is energy transfer from the QDs to MTAPc, not all the energy transferred is observed as stimulated emission, possibly due to energy loss through other processes.

The small values of r indicate that the MTAPcs are in close proximity to the donor (QDs) and thus there should be an ease of energy transfer (Eff) between the excited MPA or TGA capped QD fluorophore and the MTAPc acceptor.

Due to FRET the fluorescence quantum yield (excitation at 550 nm) of the QDs ($\Phi^{Mix}_{F(QD)}$) in the mixture with MTAPc decreased slightly, Table 7, compared to $\Phi_{F(QD)}$ of the QDs alone, indicating quenching of QD's fluorescence by MTAPc. This was noticed for both the linked and mixed MTAPc-QDs.

3.5 Fluorescence Quenching Parameters

The changes in the fluorescence emission spectra of the 3 nm CdTe-TGA QDs (1.21 mg/mL) in the presence of a range of concentrations (0 to 7.86 x 10^{-6} M, for ZnTAPc, and 0 to 4.6 x 10^{-4} M, for InTAPc) of the MTAPc are shown in Fig 28. These changes are due to the quenching of the fluorescence of the CdTe QDs by the MTAPc, due to radiationless losses of energy.

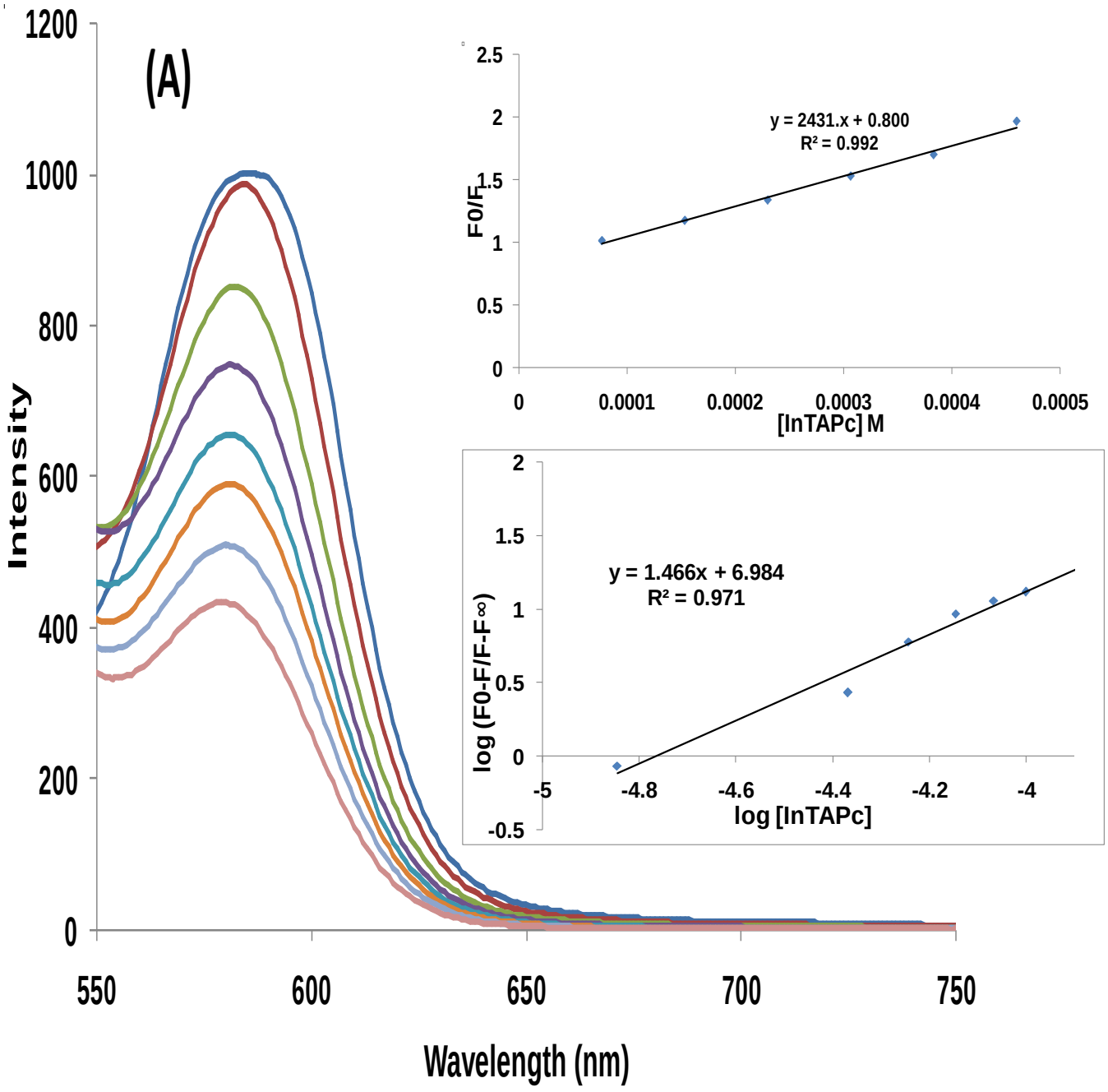
(A)
Intensity
Wavelength (nm)
1200
1000
800
600
400
200
0
550
600
650
700
750
F0/F
y = 2431.x + 0.800
R² = 0.992
[InTAPc] M
0
0.0001
0.0002
0.0003
0.0004
0.0005
0.5
1
1.5
2
2.5
log (F0-F/F-F∞)
y = 1.466x + 6.984
R² = 0.971
log [InTAPc]
-5
-4.8
-4.6
-4.4
-4.2
-4
-0.5

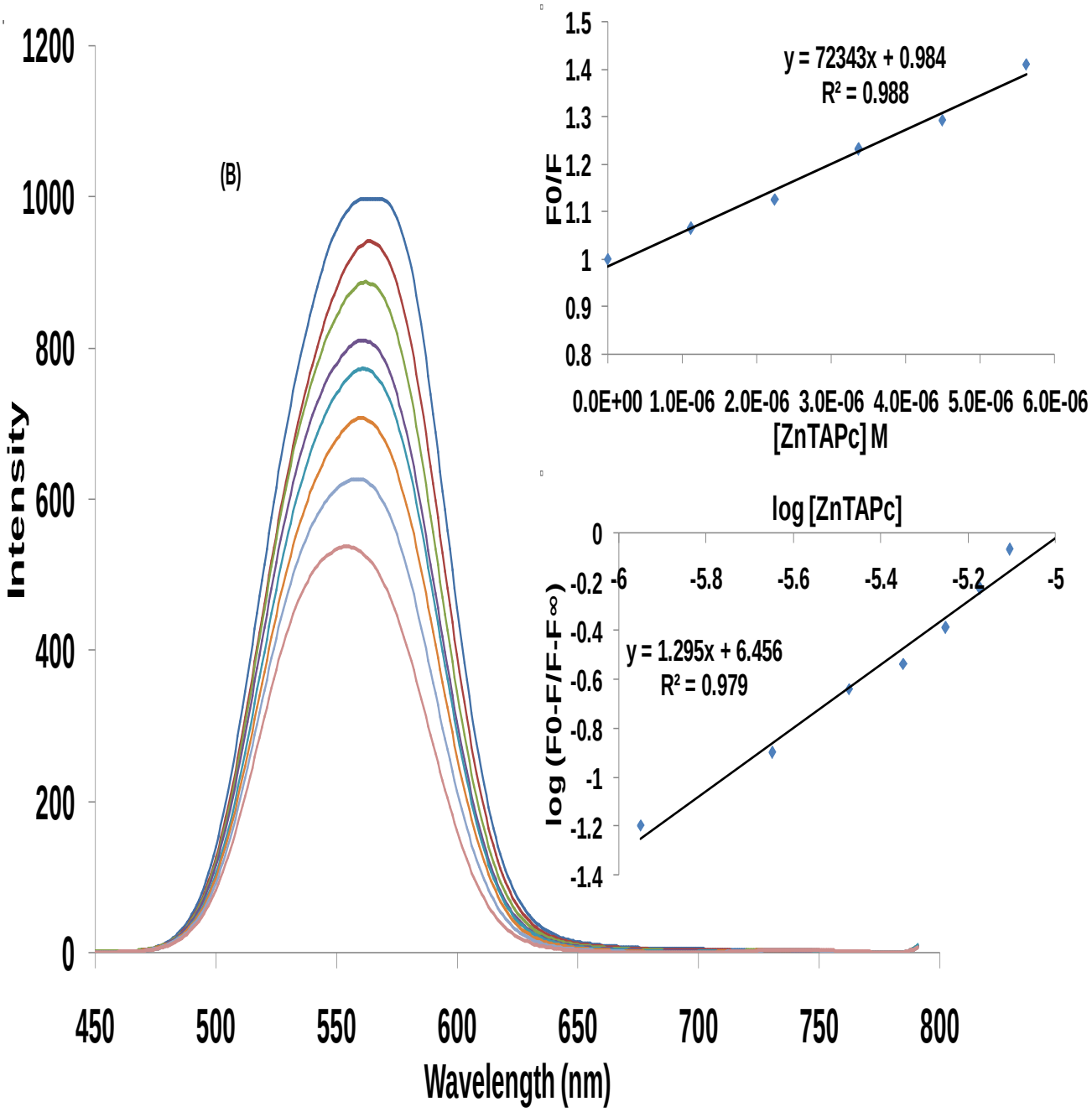

Fig. 28: Variation of the fluorescence spectra of 3 nm CdTe-TGA QDs in the presence of varying concentrations of (A) ClInTAPc, [QDs] = 1.04 mg/ml, [ClInTAPc] = 0 to 5.37 x 10^{-4} M and (B) ZnTAPc, [QDs] =1.21 mg/ml, [ZnTAPc] = 0 to 7.86 x 10^{-6} M.

Excitation 550 nm; solvent: DMF:water (3:2).

Table 7: Fluorescence quantum yields of QDs in the absence and presence of MTAPc. Solvent: DMF:water.

QDs	$\Phi_{F(QD)}$	$\Phi_{F(QD)}^{Mix}$	$\Phi_{F(QD)}^{linked}$	Size (nm)[a]
CdTe-MPA	0.163	-	-	3.0
ZnTAPc	-	0.0419	0.0111	
ClInTAPc	-	0.051	0.0137	
CdTe-MPA	0.047	-	-	3.3(3.0)
ZnTAPc	-	0.0397	0.0165	
ClInTAPc	-	0.0136	0.0031	
CdTe-TGA	0.070	-	-	3.2(3.4)
ZnTAPc	-	0.0225	0.0207	
ClInTAPc	-	0.018	0.00226	

[a] determined using equation 1. Values in brackets were determined using XRD

The QD's fluorescence was found to decrease progressively with increasing concentration of MTAPc.

A plot of $\frac{F_0}{F}$ against [MTAPc], Fig. 28 (insert), gives quenching constant (K) values (Table 8) for quenching of the QDs fluorescence in the presence of MTAPc. The linear plot obtained in Fig. 28 (inserts) confirms that the quenching equation (Eq. 10, where MPc = MTAPc) is obeyed. The value for K was found to be 72343 M^{-1} for ZnTAPc mixed with CdTe-TGA. This value (for QDs capped with TGA) is higher than the value obtained for ZnTAPc (K = 8079 M^{-1}) in the presence of the same size of QDs capped with MPA, Table 8. It is likely that since TGA is a smaller molecule than MPA, there is closer interaction of ZnTAPc for the former than the latter. K values were also determined for ClInTAPc in the presence of TGA or MPA as capping agents and the data is shown in Table 8. For ClInTAPc, the K values in the presence of TGA capped QDs is again larger than for the MPA capped QDs, due to the same reason provided above for ZnTAPc. K values were generally higher for ZnTAPc compared to ClInTAPc, hence there was less quenching of QDs by the latter. When

considering the same type of QDs, but different size QDs (e.g. ZnTAPc mixed with MPA (3.0 nm and 3.5 nm)), the larger QDs were found to give larger K values.

Table 8: Quenching and binding constants for MTAPc in the presence of QDs. Size of QDs: CdTe-MPA = 3.5 nm and 3.0nm, CdTe-TGA = 3.0 nm. Solvent = DMF:water (3:2).

Complex	K /M^{-1}	k_b /M^{-1}	n
ZnTAPc + 3nm MPA	8 079	8.77×10^8	2.4
ZnTAPc + 3nm TGA	72 343	1.26×10^8	1.3
ClInTAPc + 3nm MPA	1911	1.06×10^9	1.7
ClInTAPc + 3nm TGA	2431	2.76×10^8	1.5
ZnTAPc + 3.5nm MPA	12688	2.89×10^{10}	2.3
ClInTAPc + 3.5nm MPA	2920	4.39×10^9	1.8

The values of the binding constant obtained from the intercepts of the plots of $\log\left[\frac{(F_0-F)}{(F-F_\infty)}\right]$ vs log [MTAPc] (equation 11, with MPc = MTAPc) were of the order of 10^8 to 10^{10} M^{-1}. These values are much higher than that reported for the interaction of CdTe QDs with aluminium tetrasulfonated phthalocyanine (AlTSPc), where the values were of the order of 10^5 to 10^6 M^{-1} [39]. This could be due to different modes of interaction since AlTSPc is negatively charged while the MTAPc complexes discussed in this work are non-ionic, meaning the QD capping agent may be repelling the AlTSPc and not by the MTAPc. The number of binding sites for MTAPc on QDs as determined from insets (b) in Fig. 29 to be generally 2, except for ZnTAPc

mixed with 3.0 nm TGA QDs, which gave a binding site of 1. A value of 1 was reported before for AlTSPc on CdTe QDs [39], and the difference could be due to the nature of the MPc molecules.

3.6 Conclusion

The results presented give evidence in favour of the formation of an amide bond between MTAPc and CdTe QDs. Both the linked and mixed QDs-ZnTAPc complexes showed Förster resonance energy transfer (FRET), whereas both the mixed and linked QD-ClInTAPc complexes showed none. MTAPc quenched the QDs emission with quenching constants of the order of $10^3 – 10^4$ M^{-1}. It was also observed that the fluorescence quantum yield of QDs decreased as their size got larger. Also, the smaller QDs displayed the better FRET efficiencies in general. This is a rather unexpected result, as one would expect better efficiencies with the larger QDs, and perhaps merits some repeat investigations in order to determine whether this is an accurate reflection of what is occurring. Lastly, it was observed that the linked complexes caused a smaller induced fluorescence in the Pc component than the QD:Pc mixtures did. The reason for this is theorized to be energy lost through internal conversion within the linked complex.

The photophysical data indicates that the MTAPc studied are not very suitable for use as optical limiters due to the fact that their hyperpolarizabilities and third-order susceptibilities were too far below the optimal operating levels. The limiting intensities were very low though, which is said to be favourable, but the k values, whilst above one, were still fairly low. Again, on their own these MTAPc are not particularly good optical limiters, but it is hoped that by linking them to QDs that the optical limiting behavior may be enhanced.

References

[1] R. Bonnett, *Chemical aspects of photodynamic therapy*, Gordon and Breach Science Publishers, Germany, 2000.

[2] A. Von Braun, J. Tscheniac, *Ber. Deut. Chem. Ges*., 40 (1907) 2709.

[3] H. de Diesbach, E. von der Weid, *Helv. Chim. Acta*, 10 (1927) 886.

[4] G. T. Byrne, R. P. Linstead, A. R. Lowe, *J. Chem. Soc*, (1934) 1017.

[5] R. P. Linstead, A. R. Lowe, *J. Chem. Soc*., (1934) 1022.

[6] C. E. Dent, R. P. Linstead, *J. Chem. Soc*., (1934) 1027.

[7] J. A. Elvidge, R. P. Linstead, *J. Chem. Soc*., (1955) 3526.

[8] J. M. Robertson, *J. Chem. Soc*., (1935) 615.

[9] J. M. Robertson, *J. Chem. Soc*., (1936) 1195.

[10] J. M. Robertson, I. Woodward, *J. Chem. Soc*., (1937) 3536.

[11] C. C. Leznoff, A. B. P. Lever, *Phthalocyanines: Properties and Applications*, VCH, New York, vol 1-4 (1989 – 1996).

[12] M.P. Somashekarappa, J. Keshavayya, S. Sampath, *Pure Appl. Chem.* 74 (2002) 1609

[13] M. Gouterman, In *The Porphyrins*, (Ed. D. Dolphin), Part A. Physical Chemistry, Academic Press, New York, (1978).

[14] A. J. McHugh, M. Gouterman, C. Weiss, *Theoret. Chim. Acta,* 24 (1987), 246.

[15] A. M. Schaffer, M. Gouterman, E. R. Davidson, *Theoret. Chim. Acta,* 30 (1973), 9.

[16] M. J. Stillman, T. Nyokong, In Phthalocyanines*: Properties and Applications* (Eds. C. C. Leznoff, A. B. P. Lever, VCH, New York, (1989).

[17] G. Galli, A. Puzder, A.J. Williamson, J.C. Grossman, L. Pizzagalli, *Nanotech*. 1 (2002) 470

[18] R. E. Bailey, S.M. Nie, *J. Am. Chem. Soc.,* **125** (2003) 7100

[19] J.R. Lakowiecz, *Principles of Fluorescence Spectroscopy 2nd edn*; Kluwer Academic/ Plenum Publishers: (1999), New York

[20] S. Dayal, C. Burda, *J.Am.Chem.Soc.* 129 (2007) 7977

[21] S. Moeno, T. Nyokong, *J.Photochem.Photobiol.A: Chem.* 201 (2009) 228

[22] S. Moeno, T. Nyokong, *Polyhedron* 27 (2008) 1953

[23] A.O. Orlova, V.G. Maslov, A.V. Baranov, I. Gounko, S. Byrne, *Optics and Spectroscopy* 105 (2008) 726

[24] P. Juzenas, W. Chen, Y-P. Sun, M.A.N. Coelho, R. Generalov, N. Generalova, I.L. Christensen, *Adv. Drug Deliv. Rev.* 60 (2008) 1600

[25] P. Holister, C. Román, T. Harper, *Quantum Dots: Technology White Papers nr. 13*, Cientifica, 2003, pg. 1-7

[26] S. Dayal, R. Krolicki, Y. Lou, X. Qiu, J.C. Berlin, M.E. Kenney, C. Burda, *Appl. Phys. B* 84 (2006) 309

[27] M.E. Wieder, D.C. Hone, M.J. Cook, M.M. Handsley, J. Gavrilovic, D.A. Russel, *Photochem. Photobiol Sci.* 5 (2006) 727

[28] A.R. Clapp, I.L. Medintz, H. Mattoussi, *Chem. Phys. Chem.* 7 (2006) 47

[29] W.W. Yu, L. Qu, W. Guo, X. Peng, *Chem. Mat.* 15 (2003) 2854.

[30] J. Drbohlavova, V. Adams, R. Kizek, J. Hubalek, *Int. J. Mol. Sci.* 10 (2009) 656

[31] T. Allen, *Particle Size Measurement 3rd edn*, London: Chapman and Hall (1981)

[32] S. Brunauer, P.H. Emmett, E. Teller, *J. Am. Chem. Soc.* 60 (1938) 309

[33] C.P. Poole Jr., F.J. Owens, *Introduction to Nanotechnology*, New York: John Wiley and Sons (2003)

[34] R. Bakalova, H. Ohba, Z. Zhelev, T. Nagase, R. Jose, M. Ishikawa, Y. Baba, *Nanolett.* 4 (2004) 1567

[35] S. Fery-Forgues, D. Lavabre, *J. Chem.* 76 (1999)1260

[36] A. Ogunsipe, J-Y. Chen, T. Nyokong, *New J. Chem.* 28 (2004) 822

[37] R.F. Kubin, A.N. Fletcher, *J. Lumin.* 27 (1982) 455

[38] P. Kub'at, J. Mosinger, *J. Photochem. Photobiol. A: Chem.* 96 (1996) 93.

[39] M. Idowu, J.Y. Chen, T. Nyokong, *New J. Chem.* 32 (2008) 290.

[40] H. Du, R.A. Fuh, J. Li, L.A. Corkan, J.S. Lindsey, *Photochem. Photobiol.* 68 (1998) 141

[41] J. Rose, *Advanced Physico-chemical experiments 1st edn*; Sir Isaac Pitman and Sons Ltd, London, 1964, pg.257

[42] D. Dini, M.J.F. Calvete, M. Hanack, M. Meneghetti, *J. Phys. Chem. A* 112 (2008) 8515

[43] Y.Z. Gu, Z.J. Liang, F.X. Gan, *Opt. Mater.* 17 (2001) 471

[44] J.W. Perry, K. Mansour, S.R. Marder, D. Alvarez Jr., K.L. Perry, I. Choong, *Opt. Lett.* 19 (1994) 625

[45] C. Liu, X. Wang, G.Gong, Y. Liu, W. Qiu, D. Zhu, *Chem. Phys. Lett.* 347 (2001) 378

[46] D. Dini, M. Hanack, in: K.M. Kadish, K.M. Smith, R. Guilard (Eds.), *The Porphyrin Handbook: Physical Properties of Phthalocyanine-based Materials, vol. 17*, Academic Press, USA, 2003, p. 22.

[47] D. Dini, M. Barthel, M. Hanack*, Eur. J. Org. Chem.* (2000) 3759.

[48] Yu Chen, Michael Hanack, Yasuyuki Araki, and Osamu Ito *Chem. Soc. Rev.* **2005**, *34*, 517-529

[49] V. Chauke**,** M. Durmus, T. Nyokong, *J. Photochem. Photobiol. A: Chem.* 192 (2007) 179

[50] J. Simon, C. Sirlin, *Pure Appl. Chem.* 61 (1989) 1625.

[51] A. Auger, W. J. Blau, P. M. Burnham, I. Chambrier, M. J. Cook, B. Isare, F. Nekelson, S. M. O'Flaherty, *J. Mater. Chem*., 13 (2003) 1042.

[52] A. Shavel, N. Gaponik, A. Eychmuller, J. Phys. Chem. B**.** 110 (2006) 19280.

[53] B.N. Achar, G.M. Fohlen, J.A. Parker, J. Keshavayya, *Polyhedron*, 6 (1987) 1463

[54] P. Tau, A.O. Ogunsipe, S. Maree, D.M. Maree, T. Nyokong, *J. Porphyrins Phthalocyanine* 7 (2003) 438.

[55] M. G. Debacker, O. Deleplanque, B. Van Vlierberge, F. X. Sauvage, *Laser Chem.*, 8 (1988) 1.

[56] A. C. S. Samia, S. Dayal, C. Burda, *Photochem. Photobiol.* 82 (2006) 617.

[57] J.S. Hsiao, B.P. Krueger, R.W. Wagner, T.E. Johnson, J.K. Delaney, D.C. Mauzerall, G.R. Fleming, J.S. Lindsey, D.F. Bocian, R.J. Donohoe. *J. Am. Chem. Soc.* 118 (1996) 11181.

[58] T. Forster. *Disc. Far. Soc.* 27 (1959) 7.